

# Subsystem Density-Functional Theory (Update)

Christoph R. Jacob<sup>a,1</sup> and Johannes Neugebauer<sup>b,2</sup>

<sup>a</sup> Institute of Physical and Theoretical Chemistry, Technische Universität Braunschweig,  
Gaußstraße 17, 38106 Braunschweig, Germany

<sup>b</sup> Theoretische Organische Chemie, Organisch-Chemisches Institut, Westfälische  
Wilhelms-Universität Münster, Corrensstraße 40, 48149 Münster, Germany

Date: July 14, 2023

---

<sup>1</sup>Email: [c.jacob@tu-braunschweig.de](mailto:c.jacob@tu-braunschweig.de)

<sup>2</sup>Email: [j.neugebauer@uni-muenster.de](mailto:j.neugebauer@uni-muenster.de)

## Abstract

The past years since the publication of our review on subsystem density-functional theory (sDFT) [*WIREs Comput. Mol. Sci.* 2014, 4:325–362] have witnessed a rapid development and diversification of quantum mechanical fragmentation and embedding approaches related to sDFT and frozen-density embedding (FDE). In this follow-up article, we provide an update addressing formal and algorithmic work on FDE/sDFT, novel approximations developed for treating the non-additive kinetic energy in these DFT/DFT hybrid methods, new areas of application and extensions to properties previously not accessible, projection-based techniques as an alternative to solely density-based embedding, progress in wavefunction-in-DFT embedding, new fragmentation strategies in the context of DFT which are technically or conceptually similar to sDFT, and the blurring boundary between advanced DFT/MM and approximate DFT/DFT embedding methods.

# 1 Introduction

The subjects of contemporary chemical science move towards ever more complex structures and chemical systems [1]. Quantum Chemistry is playing an increasingly important role in the analysis and rationalization of experiments conducted on complex molecules, (bio-)polymers, molecular aggregates or materials, and molecules at interfaces. This trend is reflected in the rapidly growing activity towards quantum-chemical method development for large and complex chemical systems [2]. One attractive approach for the efficient quantum-chemical treatment of such systems are subsystem approaches, which ideally achieve a natural linear scaling with system size by partitioning a large and complex chemical system into smaller fragments [3, 4].

A particularly appealing quantum-chemical subsystem approach is provided by subsystem density-functional theory (sDFT). It achieves a partitioning in terms of the electron density, which is a measurable real-space quantity, and thus provides a chemically intuitive and versatile framework. Since the publication of our original review on sDFT in 2014 [5], the body of scientific literature either using sDFT and related methods or exploring new methodological avenues along the lines of sDFT has increased tremendously. In this Update, we provide the readership with a review of these developments and illustrate the potential of applications that have emerged in the meantime.

Subsystem density-functional theory is closely tied to the concept of density-based embedding and to theories such as Frozen-Density Embedding (FDE) [6]. Over the past years, several similar methods have emerged, which can be regarded as either technically or conceptually related. And even the formerly sharp boundary between mixed quantum chemical/classical (QM/MM) methods and density-based embedding methods of QM/QM type is fading. Thus, while our original article [5] focussed on the fundamental and applications of sDFT itself, in this Update we will broaden our perspective and also discuss

related approaches in the context of sDFT.

As this article is an Update, we will assume that readers are either familiar with or at least can familiarize themselves with the basics of sDFT and related methods as described in our original article [5]. Nevertheless, we will integrate some basic material wherever it seems necessary to keep this Update easily comprehensible.

## 2 Theoretical Background

Subsystem-DFT is based on a partitioning of the total electron density  $\rho_{\text{tot}}(\mathbf{r})$  of a complex chemical system into subsystem electron densities,

$$\rho_{\text{tot}}(\mathbf{r}) = \sum_I \rho_I(\mathbf{r}), \quad (1)$$

where each subsystem density  $\rho_I$  can be represented by a system of non-interacting particles, i.e., through the  $n_I$  occupied orbitals of the subsystem,

$$\rho_I(\mathbf{r}) = \sum_{i_I}^{n_I} |\psi_{i_I}(\mathbf{r})|^2. \quad (2)$$

Note that for a given subsystem electron density  $\rho_I(\mathbf{r})$ , the subsystem orbitals  $\{\psi_{i_I}(\mathbf{r})\}$  are implicitly determined by the requirement that they correspond to the electron density  $\rho_I(\mathbf{r})$ .

In subsystem-DFT, the total energy is then expressed as

$$E[\{\rho_I\}] = \sum_I T_s[\rho_I] + V_{\text{nuc}}[\rho_{\text{tot}}] + J[\rho_{\text{tot}}] + E_{\text{xc}}[\rho_{\text{tot}}] + T_s^{\text{nad}}[\{\rho_I\}] + V_{nn}, \quad (3)$$

where  $T_s[\rho_I]$  is the Kohn–Sham kinetic energy of subsystem  $I$ ,  $V_{\text{nuc}}[\rho_{\text{tot}}]$  is the electron–nuclei attraction energy,  $J[\rho_{\text{tot}}]$  is the Coulomb energy,  $E_{\text{xc}}[\rho_{\text{tot}}]$  is the exchange–correlation (xc) energy,  $V_{nn}$  is the nuclear repulsion energy. Finally, the non-additive kinetic energy (NAKE) is given by,

$$T_s^{\text{nad}}[\{\rho_I\}] = T_s[\rho_{\text{tot}}] - \sum_I T_s[\rho_I], \quad (4)$$

where the subsystem kinetic energies have been expressed as density functionals because the subsystem orbitals are implicitly determined by the subsystem electron densities.

Minimization of Eq. (3) with respect to the electron density  $\rho_K$  of subsystem  $K$  (subject to the condition that  $\rho_K$  can be represented by a non-interacting system with Kohn–Sham orbitals  $\{\psi_{i_K}\}$ ) while keeping all other subsystem electron densities fixed leads to Kohn–Sham-like equations for subsystem  $K$ ,

$$\left(-\frac{\nabla^2}{2} + v_{\text{eff}}^{(K)}[\rho_K](\mathbf{r}) + v_{\text{emb}}^{(K)}[\rho_K, \rho_{\text{tot}}](\mathbf{r})\right) \psi_{i_K}(\mathbf{r}) = \epsilon_{i_K} \psi_{i_K}(\mathbf{r}), \quad i = 1, \dots, n. \quad (5)$$

Here,

$$v_{\text{eff}}^{(K)}[\rho_K](\mathbf{r}) = v_{\text{nuc}}^{(K)}(\mathbf{r}) + v_{\text{Coul}}[\rho_K](\mathbf{r}) + v_{\text{xc}}[\rho_K](\mathbf{r}), \quad (6)$$

contains all the terms that would also be present in a Kohn–Sham DFT calculation for the isolated subsystem  $K$ , i.e., the nuclear potential, the Coulomb potential, and the exchange–correlation potential.

The additional embedding potential for system  $K$  is given by,

$$\begin{aligned} v_{\text{emb}}^{(K)}[\rho_K, \rho_{\text{tot}}](\mathbf{r}) &= \sum_{I, I \neq K} v_{\text{nuc}}^{(I)}(\mathbf{r}) + v_{\text{Coul}}[\rho_{\text{tot}} - \rho_K](\mathbf{r}) \\ &\quad + v_{\text{xc}}^{\text{nad}}[\rho_K, \rho_{\text{tot}}](\mathbf{r}) + v_{\text{kin}}^{\text{nad}}[\rho_K, \rho_{\text{tot}}](\mathbf{r}). \end{aligned} \quad (7)$$

The NAKE introduces a corresponding contribution to the embedding potential, the *non-additive kinetic potential* (NAKP),

$$v_{\text{kin}}^{\text{nad}}[\rho_K, \rho_{\text{tot}}](\mathbf{r}) = \frac{\delta T_s^{\text{nad}}[\{\rho_I\}]}{\delta \rho_K(\mathbf{r})} = \frac{\delta T_s[\rho_{\text{tot}}]}{\delta \rho_{\text{tot}}(\mathbf{r})} - \frac{\delta T_s[\rho_K]}{\delta \rho_K(\mathbf{r})}. \quad (8)$$

A similar nonadditive contribution  $v_{\text{xc}}^{\text{nad}}[\rho_K, \rho_{\text{tot}}](\mathbf{r})$  arises from the exchange–correlation functional.

For further details on the foundations of Subsystem-DFT and for discussions of many of the subtleties in defining the required density functionals and their functional derivatives, we refer to our original article [5] as well as the references cited therein.

In practical calculations, the theory presented above can be applied in two different ways, either as a subsystem method for treating a large system efficiently (i.e., the target is the full system and all subsystems are treated on an equal footing) or as an embedding method (i.e., the target is one specific subsystem, which is embedded in an environment composed of all other subsystems). The former case is typically known as Subsystem-DFT (sDFT). Here, all subsystem electron densities  $\rho_I(\mathbf{r})$  are optimized iteratively, either sequentially in freeze-and-thaw iterations or simultaneously. In the latter case, the electron density of the environment is kept frozen, and only the electron density of the active subsystem is optimized. This case is commonly referred to as Frozen Density Embedding (FDE). For extensive discussion of its theoretical foundations, we refer to Ref. 7 as well as the recent work in Refs. 8,9.

### 3 Overview of Recent Developments in Subsystem Density-Functional Theory

Since our original review [5], the field of Subsystem-DFT (sDFT) and Frozen-Density Embedding (FDE) has grown tremendously. Other general overviews that have been published in the meantime include a review of multilevel electronic-structure simulation methods based on FDE by Wesolowski *et al.* [7]. A special issue of the *International Journal of Quantum Chemistry* was devoted to quantum embedding electronic-structure methods; the content is summarized in the editorial in Ref. 4. Recently, König and coworkers reviewed sDFT and FDE in comparison to classical polarizable embedding schemes [10].

Density-based embedding and sDFT implementations are more and more easily accessible, either in well-established major quantum chemistry packages or in rather new, often open-source implementations focussing on these types of approaches. Concerning papers giving

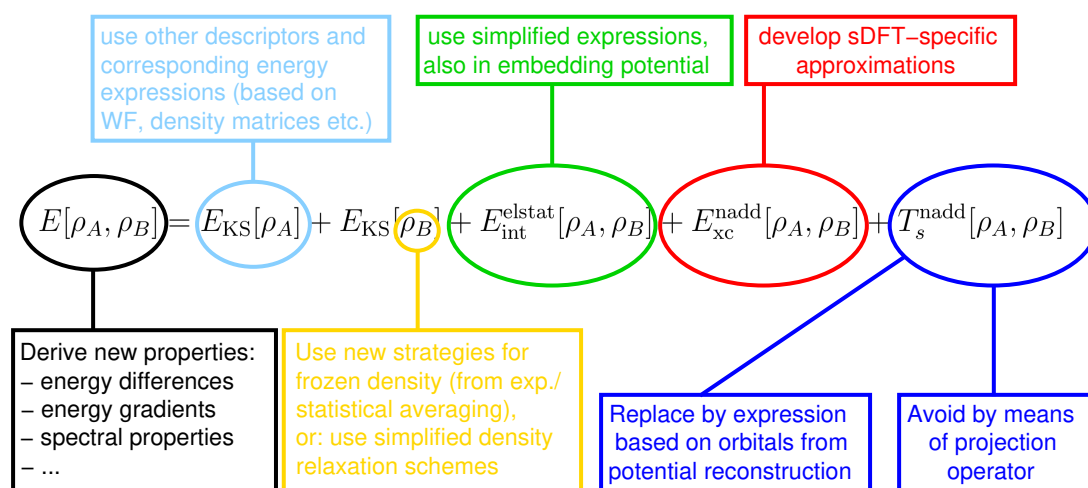


Figure 1: Overview of different aspects of sDFT/FDE that have been addressed in the past decade. The equation shown corresponds to Eq. ( ) for the case of two subsystems ( $A$  and  $B$ ), reformulated to highlight the subsystem framework (i.e., the total energy is given as a sum of Kohn–Sham energy expressions for the two subsystem densities plus electrostatic, exchange–correlation, and non-additive kinetic terms mediating the interaction).

an overview over specific software implementations of sDFT and related methods since 2014, we mention the papers describing the SERENITY subsystem quantum chemistry program [11,12], the eQE package [13,14], CP2K [15,16], KOALA [17], and TURBOMOLE [18,19]. The related projection-based embedding (see Section 6.1) is also available in MOLPRO [20] and Q-CHEM [21].

Overall, the boundaries between sDFT/FDE and other subsystem and embedding methods become have become more blurry in recent years. A broader comparison of general embedding and fragmentation approaches is presented in Ref. 22. Sun and Chan provided a comparative overview over density, Green’s function, and density-matrix embedding theories [23], and a broader perspective on both QM/MM and QM/QM embedding methods, including density-based ones, has been provided by Jones *et al.* [24]. In this Update, we review recent developments in the field of density-based subsystem and embedding methods. Here, we start from the perspective of sDFT/FDE and discuss work that was been published in the past decade along different lines (for an overview, see Fig. 1).

First, recent developments related to fundamental aspects are discussed in Section 4. Here, the most relevant aspect is the treatment of the NAKE and the associated NAKP, and novel developments of approximations for these are presented in Section 4.1. The treatment of the non-additive exchange–correlation energy (NAXC) has also attracted some interest, and strategies for approximating the NAXC energy in the case of non-local xc-functionals and for improving upon conventional xc approximations within sDFT are discussed in Section 4.2. The use of potential reconstruction techniques in order to avoid approximations for the NAKE altogether are presented in Section 4.3. Surveys of further fundamental aspects related to sDFT/FDE can be found in our original article [5] and in the review by Wesolowski and coworkers [7]. An instructive comparative discussion of the fundamentals of sDFT/FDE in relation to other density-based subsystem and embedding approaches is provided by Pavanello and coworkers (see Table 1 in Ref. 25). For recent development in partition DFT, which shares several features with sDFT but allows for fractional numbers of electrons per subsystem and enforces a common embedding potential for all subsystems, we refer to the work of Wasserman and coworkers [26–34]. Finally, the use of sDFT/FDE for accessing specific spin states and broken-symmetry sDFT approaches are presented in Section 4.4. A related review of developments and applications of sDFT/FDE for spin densities and spin-related properties is given in Ref. [35]

Second, applications of sDFT/FDE cover a wide range of different types of chemical systems, and specific variants and extensions have been developed that are tailored to certain types of applications. These will be covered in Section 5. Most importantly, there is a continuum between sDFT, in which all subsystems are treated at the same footing, and FDE, in which one focusses on one specific subsystem of interest. In the latter case, numerous strategies are available for choosing the frozen electron densities. Moreover, sDFT/FDE can be further combined with other embedding approaches in sophisticated multilevel schemes.

Applications of sDFT to molecular dimers and clusters are reviewed in Sections 5.1 and 5.2, respectively. The use of FDE for modeling solvent effects on molecular properties and novel strategies for choosing the frozen electron densities of the solvent in such studies are discussed in Section 5.3. Novel developments for applying sDFT/FDE to a wide variety of bulk systems — including liquids and solids — as well as their interfaces are presented in Section 5.4. For an earlier review on sDFT advances for condensed-phase systems, including aspects of excited states, dynamics, and many-body interactions, we also refer to Ref. 25. Applications of FDE for local impurities in bulk systems and for molecules adsorbed on surfaces are reviewed in Section 5.5. Finally, extensions for applying sDFT/FDE to biomolecules are discussed in Section 5.6.

Third, a wide range of extensions of sDFT/FDE is reviewed in Section 6. Major developments in recent years have addressed the replacement of NAKE approximations by projection techniques. An account of projection-based embedding (PbE), which can be regarded as a variant of density-based embedding with mutually orthogonal subsystem orbitals, in combination with correlated-wavefunction descriptions of the active system has been given by Manby, Miller and co-workers [36]. Applications of PbE for transition metal complexes have been reviewed in Ref. 37. Here, we will discuss PbE techniques and their relation to sDFT in Section 6.1.

Extensions of sDFT/FDE for the treatment of excited states are covered in Section 6.2. Besides new insights into fundamental aspects of the treatment of excited states with sDFT, these include the description of excited-state phenomena strongly sensitive to environmental and/or aggregation effects. Diabatization methods for charge- and spin-localized states based on sDFT are reviewed in Section 6.3.

Recent work concerning the extension of sDFT/FDE for the calculation of response properties, such as optical rotation dispersion (ORD) are discussed in Section 6.4, and extensions to magnetic properties, most importantly nuclear magnetic resonance (NMR) and

electron paramagnetic resonance (EPR) are reviewed in Section 6.5.

Another vast field that has grown rapidly in the past decade is the combination of density-based embedding with correlated wavefunction methods. Novel developments include accounting for ever more sophisticated interactions, and the use of more and more accurate types of wavefunction methods. Libisch, Huang, and Carter have discussed theory and applications of embedded correlated wavefunction methods, making use of a density-based embedding potential derived from potentially periodic environments [38]. Another review by Carter and co-workers provided an overview of density-functional and potential-functional embedding [39]. Different perspectives on wavefunction-in-DFT embedding have been discussed in Ref. 40. Here, we will review the developments in wavefunction-in-DFT embedding in Section 6.6.

While most of the work reviewed in this Update addresses non-relativistic theory, we note that an FDE implementation within the framework of the full four-component relativistic Dirac–Kohn–Sham Theory was recently presented in Ref. 41.

## 4 Fundamentals of Subsystem-Density Functional Theory

### 4.1 Non-additive Kinetic Energy

#### 4.1.1 Decomposable Approximations

The accuracy of sDFT/FDE calculations in practice hinges on the approximations used for the non-additive kinetic-energy functional [Eq. (4)] and the corresponding potential [Eq. (8)]. Most commonly, *decomposable approximations to the NAKE* are employed,

which are based on an approximate, explicitly density-dependent kinetic-energy density functional  $\tilde{T}_s[\rho]$ , i.e.,

$$\tilde{T}_s^{\text{nad}}[\{\rho_I\}] = \tilde{T}_s[\rho_{\text{tot}}] - \sum_I \tilde{T}_s[\rho_I] \quad (9)$$

with the corresponding NAKP

$$\tilde{v}_{\text{kin}}^{\text{nad}}[\rho_K, \rho_{\text{tot}}](\mathbf{r}) = \frac{\delta \tilde{T}_s^{\text{nad}}[\{\rho_I\}]}{\delta \rho_K(\mathbf{r})} = \frac{\delta \tilde{T}_s[\rho_{\text{tot}}]}{\delta \rho_{\text{tot}}(\mathbf{r})} - \frac{\delta \tilde{T}_s[\rho_K]}{\delta \rho_K(\mathbf{r})}. \quad (10)$$

Many such kinetic-energy density functionals (KEDF) have been developed for exploring orbital-free DFT as an efficient alternative to Kohn–Sham DFT (for recent work, see, e.g., Refs. 42–54). In our original article [5], we reviewed the KEDFs available at that time and their use as basis for decomposable approximations in the context of sDFT and FDE, with a focus on generalized-gradient approximation (GGA) KEDFs,

$$\tilde{T}_s^{\text{GGA}}[\rho] = C_{\text{TF}} \int \rho^{5/3}(\mathbf{r}) F(\rho(\mathbf{r}), \nabla \rho(\mathbf{r})) \text{d}\mathbf{r}. \quad (11)$$

Here, numerous forms are available for the enhancement factor  $F(\rho, \nabla \rho)$  (see Table 1 in Ref. 5). To date, such GGA KEDFs are still most widely used in applications of sDFT and FDE, in particular the PW91k (also known as LC94) [55] and the revAPBEK [56] functionals (see also Section 5.1 below). The latter has been found to be more accurate than all other available GGA KEDFs in sDFT/FDE calculations in Ref. 56, and it was found to be superior to PW91k for sDFT simulations of periodic systems by Pavanello and coworkers [57].

In recent years, there has also been some interest in specifically developing KEDFs for sDFT and FDE. Grimm and Visscher [58] revisited GGA functionals in FDE and re-optimized the parameters of a family of PBE-like KEDFs for excitation energy shifts in bimolecular complexes. They found that such a re-parametrization does not improve with respect to other GGA functionals and that the local-density Thomas–Fermi functional provides results of similar accuracy. They concluded that there is not much room for improvement within the class of GGA KEDFs.

The group of Della Sala has explored the use of post-GGA KEDFs in sDFT. They considered functionals depending on the Laplacian of the electron density,

$$\tilde{T}_s^{\text{Lapl}}[\rho] = C_{\text{TF}} \int \rho^{5/3}(\mathbf{r}) F\left(\rho(\mathbf{r}), \nabla\rho(\mathbf{r}), \nabla^2\rho(\mathbf{r})\right) d\mathbf{r}. \quad (12)$$

When considering kinetic-energy functionals based on a (modified) fourth-order gradient expansion [59] in sDFT calculations, they found that these perform well for the interaction energies and electron densities of non-covalent complexes, but do not offer a clear improvement compared to GGA KEDFs.

Beyond GGA KEDFs, nonlocal KEDF have been rather successful for the orbital-free DFT treatment of specific classes of metals and semiconductors (for a review, see, e.g. Ref. 45). Thus, exploring such non-local KEDF in decomposable approximations to the NAKE in sDFT/FDE appears to be a promising avenue. These nonlocal KEDFs are of the form,

$$\tilde{T}_s^{\text{non-local}}[\rho] = \tilde{T}_s^{\text{TF}}[\rho] + \tilde{T}_s^{\text{vW}}[\rho] + \tilde{T}_s^{\text{NL}}[\rho]. \quad (13)$$

where  $\tilde{T}_s^{\text{TF}}[\rho]$  and  $\tilde{T}_s^{\text{vW}}[\rho]$  are the Thomas–Fermi and von Weizsäcker KEDFs, respectively, and  $\tilde{T}_s^{\text{NL}}[\rho]$  is of the form,

$$\tilde{T}_s^{\text{NL}}[\rho] = \int \rho(\mathbf{r})^\alpha \omega_{\text{TNL}}[\rho](\mathbf{r}, \mathbf{r}') \rho(\mathbf{r}')^\beta d\mathbf{r} d\mathbf{r}', \quad (14)$$

where  $\omega_{\text{TNL}}[\rho](\mathbf{r}, \mathbf{r}')$  is the kernel of the non-local functional while  $\alpha$  and  $\beta$  are positive exponents. Commonly, the linear response of the electron gas, which is described analytically by the Lindhard function, is used as exact constraint in the construction of such KEDFs. This non-local part can be evaluated efficiently in reciprocal space [where the kernel becomes  $\omega_{\text{TNL}}[\rho](q)$ ], which currently limits the applicability of non-local KEDFs to periodic systems.

While most available non-local KEDFs [48, 60] employ a kernel that only depends on the average electron density,  $\omega_{\text{TNL}}(\rho_{\text{avg}})(q)$ , Mi and Pavanello [49] developed a non-local KEDF

with a kernel depending on the local electron density at each point in space (analogous to the local density approximation),  $\omega_{\text{TNL}}(\rho(\mathbf{r}))(\mathbf{r}, \mathbf{r}')$ , and proposed a protocol for evaluating the resulting KEDF efficiently. Their non-local functional, dubbed LMGP, is constructed from first principles (i.e., without empirical parameters) such that it shows the correct asymptotic of the corresponding potential, and by virtue of its locally density-dependent kernel it is able to account for large density inhomogeneities. In orbital-free DFT calculations, LMGP shows excellent performance for finite clusters and quantum dots. The non-local LMGP functional has been adapted for application in a decomposable approximation to the NAKE [61], and it was shown that it outperforms GGA NAKes for the interaction energies and electron densities of noncovalent complexes.

Because of their formulation in reciprocal space, the application of non-local KEDFs for molecular systems in non-periodic implementations is rather cumbersome. Therefore, Sarcinella *et al.* [62] introduced the reduced Yukawa potential,

$$y_{\alpha}(\mathbf{r}) = \frac{3\pi\alpha^2}{4k_F(\mathbf{r})} \int \frac{\rho(\mathbf{r}')e^{-\alpha k_F(\mathbf{r})|\mathbf{r}-\mathbf{r}'|}}{|\mathbf{r}-\mathbf{r}'|} d^3r' \quad (15)$$

as an additional ingredient for KEDFs formulated in real space. In Eq. (15),  $\alpha$  is an adjustable parameter and  $k_F(\mathbf{r}) = (3\pi^2\rho(r))^{1/3}$  is the Fermi wave vector. Using the reduced Yukawa potential, they developed non-local KEDFs in real space of the GGA-like form,

$$\tilde{T}_s^{\text{Lapl}}[\rho] = C_{\text{TF}} \int \rho^{5/3}(\mathbf{r}) F(\rho(\mathbf{r}), \nabla\rho(\mathbf{r}), \nabla^2\rho(\mathbf{r}), y_{\alpha}(\mathbf{r})) d\mathbf{r}. \quad (16)$$

They showed that such functional are able to accurately model the linear response of the electron gas and obtained promising results for rare-gas atoms as well as jellium clusters. Recently, they proposed an expansion of the Yukawa kernel in Eq. 15 in terms of Gaussian functions in order to facilitate an implementation in quantum-chemical program packages using Gaussian-type orbitals as basis functions [63].

### 4.1.2 Non-decomposable approximations

A second class of approximations to the NAKE and the NAKP are *non-decomposable* approximations, which do not rely on a parent KEDF, but set out to approximate  $\tilde{T}_s^{\text{nad}}[\{\rho_I\}]$  (or its functional derivative) directly. Early non-decomposable approximations addressed the observation that at the frozen subsystem, the NAKP should fully cancel the attractive nuclear potential, and that GGA KEDFs fail to achieve this [64]. Thus, in Ref. 64 a non-decomposable correction to the NAKP was proposed by one of us to enforce the correct behavior in regions in which the active electron density is negligible compared to the frozen electron density.

In a similar spirit, Garcia-Lastra and Wesolowski constructed a non-decomposable approximation, dubbed NDSD, that switches between the Thomas–Fermi NAKP and the von Weizsäcker NAKP [65]. The latter is switched on in the vicinity of the nuclei of the frozen subsystems, where it shows the correct behavior and cancels out the Coulomb potential of the nucleus. The switching function used in NDSD uses the reduced density gradient of the frozen electron density to detect regions close to the nuclei. Recently, Wesolowski and co-workers improved on this functional by considering a more general kernel of a differential operator instead of the von Weizsäcker functional and by improving the switching function, resulting in the non-decomposable NDCS approximation [66] as well as a symmetrized version thereof [67].

Inspired by the success of non-local KEDFs in sDFT, Shao, Mi, and Pavanello (SMP) developed a GGA-level non-decomposable NAKE functional that mimics the behavior of those non-local functionals [68]. They realized that in non-local KEDFs (see Eq. 13), the non-local part cancels out the Thomas–Fermi contribution in low-density regions (resulting in a GGA-like behavior in these regions), whereas it cancels the von Weizsäcker contribution in high-density regions (resulting in a Thomas–Fermi-like behavior in these regions). In addition, they noted that considering the regions of large inter-subsystem

overlap is crucial for accurate NAKE approximations. Based on these observations, they constructed a non-decomposable NAKE approximation that switches between Thomas–Fermi in regions where the electron density is large compared to the inter-subsystem overlap regions and the revAPBE GGA KEDF in regions where the electron density is small compared to the inter-subsystem overlap regions. The resulting (non-decomposable) SMP approximation is shown to achieve excellent accuracy for interaction energies in noncovalent complexes.

An interesting non-decomposable NAKE approximation was proposed by Wasserman and co-workers [69]. It is based on a two-orbital approximation (2OA) that assumes that the electron densities of the active and the frozen subsystem are each two-electron (one-orbital) densities (for which the von Weizsäcker functional is applicable) and that the total electron density is a two-orbital density consisting of a gerade and an ungerade orbital. They showed that after an empirical scaling, such a 2OA performs surprisingly well for rare-gas dimers.

## 4.2 Non-additive Exchange–Correlation Energy

In analogy to the kinetic energy, the exchange–correlation energy in Eq. (3) can be expressed as

$$E_{\text{xc}}[\rho_{\text{tot}}] = \sum_I E_{\text{xc}}[\rho_I] + E_{\text{xc}}^{\text{nad}}[\{\rho_I\}] \quad (17)$$

with the non-additive xc energy (NAXC)

$$E_{\text{xc}}^{\text{nad}}[\{\rho_I\}] = E_{\text{xc}}[\rho_{\text{tot}}] - \sum_I E_{\text{xc}}[\rho_I]. \quad (18)$$

The functional derivative of the NAXC leads to the corresponding non-additive xc potential,

$$v_{\text{xc}}^{\text{nad}}[\rho_K, \rho_{\text{tot}}](\mathbf{r}) = \frac{\delta E_{\text{xc}}[\rho_{\text{tot}}]}{\delta \rho_{\text{tot}}(\mathbf{r})} - \frac{\delta E_{\text{xc}}[\rho_K]}{\delta \rho_K(\mathbf{r})} \quad (19)$$

in the embedding potential for subsystem  $K$  [cf. Eq. (7)].

If the xc energy is approximated using the local-density approximation (LDA) or a generalized gradient approximation (GGA) functional, the NAXC contributions can be handled consistently in sDFT, i.e., no additional approximations need to be introduced for these terms compared to a supermolecular KS-DFT treatment [70]. Nevertheless, sDFT can be exploited to apply different xc approximations for different subsystems, and another approximation can be chosen for the NAXC [71]. In particular, the use of hybrid functionals as well as orbital-dependent localized Hartree–Fock was explored by Della Sala and coworkers [72–74].

Once xc approximations are used that depend not only on the electron density, but also on the occupied (and possibly also the virtual) KS orbitals, the first term in Eq. (18) is not accessible anymore in sDFT, and additional approximations need to be introduced for the NAXC. If hybrid or meta-GGA functional are used for the subsystems, one commonly applies a GGA for the NAXC and the corresponding potential [72,74]. We note, however, that these restrictions do no longer apply in the case of projection-based embedding (see Section 6.1).

For meta-GGAs, which depend on the occupied orbitals via the Kohn–Sham kinetic-energy density, with  $\tau^{\text{KS}}(\mathbf{r}) = \frac{1}{2} \sum_i |\nabla\psi_i(\mathbf{r})|^2$ , Della Sala and coworkers have developed dedicated approximations for the NAXC. These rely on a model of  $\tau^{\text{KS}}(\mathbf{r})$  as an explicit functional of the local electron density. Initially, they explored the use of linear combinations of the Thomas–Fermi and von Weizsäcker kinetic-energy densities as well as the kinetic-energy density of the revAPBEK approximation in combination with a Laplacian-dependent term [75]. They found that such NAXC approximations clearly improve compared to the use of a GGA for the NAXC. Subsequently, they proposed a Laplacian-dependent model of the form  $\tau^{\text{KS}} \approx \tau^{\text{TF}} (1 + as + bq)$ , where  $s$  is the reduced density gradient,  $q$  is the reduced Laplacian, and  $a$  and  $b$  are optimized parameters [76]. For sDFT with meta-GGA xc functionals, this model was found to be superior to all

previous approximations.

The partitioning of the electron density into subsystems that is provided by sDFT can also be used to address known shortcomings of existing approximations to the xc functional, most importantly the self-interaction error that leads to an over-delocalization of electron densities. First, this error can be reduced by enforcing a particular distribution of the electrons, i.e., the assignment of the electrons to localized subsystems avoids spurious delocalization. It was shown that this effect leads to an improved description of liquid water and of hydroxyl radicals in aqueous solution [77] (see also Section 5.4). Similarly, it allows for the treatment of open-shell subsystems to arbitrary local-spin patterns (see Section 4.4) and to obtain quasi-diabatic states (see Section 6.3). Second, if one allows for fractional electron numbers in the subsystems [78], the intermolecular self-interaction error can be specifically addressed by enforcing the correct fractional-charge behavior of the subsystem energies [79]. To this end, our (CRJ's) lab developed a scheme in which the subsystem energies at fractional electron numbers are calculated as linear interpolation between those obtained at integer electron numbers, i.e.,

$$E_I[\rho_I^{N_I+q}] = (1 - q)E_I[\rho_I^{N_I}] + qE_I[\rho_I^{N_I+1}], \quad (20)$$

where the superscript specifies the number of electrons in the subsystem, with the integer  $N_I$  and a fractional charge  $0 \leq q \leq 1$ . Note that this scheme is inspired by Wasserman's partition DFT [32], but treats the NAXC using a conventional GGA functional. For the prototypical tetrathiafulvalene–tetracyanoquinodimethane (TTF–TCNQ) complex, it could be demonstrated that such an approach leads to a correct description of the intermolecular charge transfer induced by an electric field.

Finally, the combination of approximate NAKE and NAXC functionals can result in error compensation that can lead to an improved agreement of sDFT with high-level reference calculations. This has been explored in several studies, which will be discussed below in Section 5.1.

### 4.3 Avoiding approximate NAKE functionals by potential reconstruction

Especially for strongly interacting subsystems, the use of approximations for the NAKE and the NAKP often leads to deteriorated results. Hence, there has been considerable interest in getting highly accurate or even exact reference results for the embedding potentials in such calculations over the past years. These are based on the realization that the functional derivative of the noninteracting kinetic energy functional, evaluated for the electron density  $\rho(\mathbf{r})$ , can be expressed as [80],

$$\frac{\delta T_s[\rho]}{\delta \rho(\mathbf{r})} = -v_s[\rho](\mathbf{r}) + \mu. \quad (21)$$

Here,  $v_s[\rho]$  is the local potential that has the target density  $\rho(\mathbf{r})$  as its non-interacting ground state, and the chemical potential  $\mu$  introduces only a constant shift. Therefore, the NAKP [Eq. (8)] can be obtained as [64],

$$v_{\text{kin}}^{\text{nad}}[\rho_K, \rho_{\text{tot}}](\mathbf{r}) = v_s[\rho_K] - v_s[\rho_{\text{tot}}] + \Delta\mu. \quad (22)$$

Thus, up to the constant shift  $\Delta\mu = \mu_{\text{tot}} - \mu_K$ , the NAKP can be obtained by reconstructing both the local potential yielding the total density,  $v_s[\rho_{\text{tot}}]$ , and one yielding the density of the active subsystem,  $v_s[\rho_K]$ . This approach has already been discussed in detail in our original article [5]. In the following, we review work related to this field from the past eight years.

Several new and improved methods have been developed for the reconstruction of local potentials from electron densities (i.e., for the inversion of the Kohn–Sham equations), possibly also using orbitals, density matrices or wavefunctions [81–94]. For an overview and discussions of successes and challenges, we refer to the reviews by Wasserman and coworkers [95, 96]. The application of potential reconstruction algorithms in sDFT was reviewed by Banafsheh and Wesolowski [97]

A comparative analysis of several reconstruction techniques for use in sDFT/FDE [98] revealed a number of interesting conclusions for practical applications. In particular, it turned out that the residual density error of typical standard reconstruction schemes can be reduced by combining them. For instance, combining a first reconstruction step with an efficient basis-set representation of the reconstructed potential with a numerically more flexible grid-based scheme considerably reduced the resulting error. Moreover, a comparison of top-down reconstruction, in which a supersystem calculation is needed as a reference, and bottom-up reconstruction, in which the supersystem density is obtained as a sum of subsystem densities, was carried out in that work. It could be concluded that bottom-up embedding typically leads to more accurate results for densities, but is less robust for more strongly interacting systems, where top-down embedding is preferable. Another conclusion was that performing potential reconstruction both for the supersystem and for the subsystems to calculate the embedding potential often results in error cancellation rather than error accumulation.

A first area of application for potential reconstruction schemes in sDFT is the development of approximate NAKE functionals. Here, the reconstruction of the NAKP using Eq. (22) can provide valuable reference data to guide the construction of approximations [99]. Following up on earlier work [100,101], Wesolowski and coworkers investigated the case of weakly overlapping pairs of two-electron densities, for which an analytic inversion of the Kohn–Sham equations is possible. Wasserman and coworkers applied numerical inversion techniques to provide accurate reference data for the NAKE in covalently bound diatomic molecules [102] as well as rare gas dimers [69]. In the latter work, this reference data was used for the (re-)parametrization of approximate kinetic energy and NAKE functionals.

Second, potential reconstruction schemes can be used to study fundamental aspects of sDFT/FDE. Because of a claim in the literature suggesting that sDFT can formally only be exact if the orbitals of different subsystems are mutually orthogonal [103], which was

picked up also in later work [104,105], our groups used potential reconstruction techniques to obtain accurate reference potentials for molecular sDFT calculations with finite basis sets [106]. Together with analytical examples and basis-set-free numerical calculations, these computations proved that there is no need for requiring this so-called external orthogonality in sDFT calculations. Nevertheless, external orthogonality (EO) — which is effectively equivalent to projector-based embedding (see Section 6.1) — can be used in density-based embedding as a workaround, i.e., *instead of* non-additive kinetic-energy approximations.

Third, potential reconstruction techniques can be used in cases where the required supermolecular DFT calculation and the corresponding potential reconstruction are not the main computational bottleneck. For instance, an application of potential reconstruction to calculate electronic excitation energies in micro-solvated systems has been presented by our groups in Ref. 107. By correcting the errors introduced in terms of an approximate NAKP, it could be shown that excitation energies are considerably improved especially for short solute–solvent distances. These uncoupled FDE-TDDFT calculations (see also Section 6.2.2) represent a case in which potential reconstruction can in fact lead to an improved efficiency compared to supersystem Kohn-Sham calculations — despite the necessity to perform a demanding supersystem potential reconstruction. Efficiency is gained if the TDDFT part of the calculation becomes the bottleneck, since the uncoupled FDEu-TDDFT calculations can be performed in a subsystem (monomer) basis. This, together with the fact that low-cost adiabatic local-density approximation (ALDA) kernels are sufficiently accurate in this context, can make the post-SCF part of the calculation very fast compared to the supersystem calculation. Similar efficiency arguments apply if potential reconstruction is combined with WF-in-DFT embedding strategies, which are discussed below in Section 6.6.

Closely related to sDFT/FDE making use of potential reconstruction are the density and

potential functional embedding theories (DFET, PFET) developed mainly by the Carter group [108,109]. DFET can be regarded as an FDE variant making use of potential reconstruction (specifically: Wu–Yang-type reconstruction [110]) and additionally introducing the constraint of a common embedding potential for all subsystems [39]. Once the embedding potential is optimized based on embedded DFT calculations for the subsystems, it can also be combined with correlated wavefunction-type subsystem calculations in this framework. In PFET, by contrast, also electron densities for subsystems from correlated wavefunction calculations can be employed to construct input densities for the potential-reconstruction procedure [39]. An implementation of DFET in the framework of the projector-augmented-wave method has been presented in 2015 [111]. Technical challenges associated with the combination of periodic DFT codes and molecular electronic-structure programs have been addressed in Ref. 16, where the embedding potential is expanded in terms of basis-function products (rather than AO basis functions only). A PFET implementation that allows to use mixed correlated wavefunction/DFT setups has been described in Refs. 112,113. Later, the method has been generalized to a density-matrix functional embedding making use of non-local embedding potentials to improve the description of fragments connect through covalent bonds [114]. As an alternative, DFET has been combined with a capped-fragment scheme in Ref. 115, which shares several features with the 3-FDE method [116]. Hoyer *et al.* have presented an extension to embed a subsystem described with a non-collinear two-component electronic-structure method in an environment treated with a collinear approximation [117]. A finite-temperature version of DFET was proposed by Huang [118] and later on used in the framework of an embedded cluster density approximation for the exchange–correlation energy [119–122]. As an alternative to avoid dangling bonds for covalently bonded subsystems, Huang *et al.* also proposed a link-atom-style partitioning of each boundary atom into two atoms for which the sum of the (valence) electrons equals that of the corresponding boundary atom [123]. The DFET strategy has also been employed for patching exchange–correlation potentials

based on correlated wavefunction calculations for subsystems inside a larger system [124].

#### 4.4 Broken-Symmetry sDFT and Access to Spin States

A big advantage of sDFT in practical calculations is that charge and spin state of every subsystem can be specified by the user. This can be used, for instance, to converge aggregates of open-shell subsystems to arbitrary local-spin patterns in an almost trivial manner [125]. In KS-DFT calculations, this often causes problems either due to the overdelocalization error or simply due to problems to converge to a desired spin distribution.

But while the spin densities of such sDFT calculations often have all the desired features, the magnetic exchange coupling constants that can be extracted based on a broken-symmetry-like treatment from the energy difference of a high-spin and a broken-symmetry occupation pattern turned out to be disappointing when standard NAKE approximations are used. For proper energetics and exchange couplings, techniques of potential reconstruction can be applied, which give access to a set of supersystem orbitals and the corresponding accurate non-additive kinetic energy [125]. In subsequent work, it was confirmed that the essential ingredient to get at least semi-quantitative exchange couplings is in fact the evaluation of the non-additive kinetic energy based on a set of orthogonal orbitals characterizing the supersystem [126]. In that study, these orbital sets were constructed by simple combination and mutual orthogonalization of the subsystem orbitals in a pragmatic approach. While this brings the exchange couplings into the right order of magnitude, it at the same time also introduces an undesirable basis-set dependence.

# 5 Applications of Subsystem Density-Functional Theory and Frozen-Density Embedding

## 5.1 Molecular Dimers

Complexes of non-covalently bonded molecules, typically dimers, present an ideal test case for sDFT. By comparing the results obtained in a supermolecular calculation to a sDFT calculation in which each molecule is treated as a separate subsystem, one can directly assess the errors introduced by the sDFT treatment. If a semilocal XC functional is used in the supermolecular KS-DFT calculation, the NAXC can be handled consistently. By further ensuring that a supermolecular basis set is used in the sDFT calculation, the remaining errors can be traced back to the NAKE approximation [70].

Several test sets of molecular dimers have been employed in studies of novel NAKE approximations (see Section 4.1). Typically, in such studies interaction energies and/or properties derived from the electron density are considered. Unfortunately, there are no well-established benchmarks sets, and the results available in the literature are therefore rather diverse and not always consistent (see, e.g., Refs. 56, 57, 59, 65, 66, 68, 76, 127). A rather extensive test set consisting of 40 molecular dimers has been used by Della Sala in Ref. 76, partly based on earlier work [78, 128–132]. It consists of seven weakly interacting complexes (such as rare gas dimers, six dimers featuring dipole–dipole interactions (such as the HCl and H<sub>2</sub>S dimers), six hydrogen-bonded complexes (such as the water dimer) as well as eight complexes with a noncovalent hydrogen–hydrogen bond (such as LiH–HF), and twelve charge-transfer complexes (such as NF<sub>3</sub>–HCN). For this test set, both interaction energies and electron densities resulting from sDFT calculations were compared to assess the accuracy of NAKes. Wesolowski and coworkers used different test sets consisting of combinations of ions (such as Li<sup>+</sup>, Mg<sup>2+</sup>, O<sup>2-</sup>) and rare gas atoms or

small molecules (such as water and HF) in Refs. 65, 66. Existing benchmark sets for intermolecular interactions, in particular the S22 [133], S22-5 [134], and S66 [135] as well as the A24 [136] test sets have also been investigated in the context of sDFT [61, 68, 127, 137].

Besides electron densities and interaction energies, the correct description of potential-energy curves of non-covalently bound complexes is of particular interest. Obviously, the accuracy — both compared to supermolecular KS-DFT and to high-level reference data — will be determined by the approximations used for the NAXC and NAKE. The potential-energy surface of the water dimer was revisited by Genova *et al.* [77]. They found that with both PBE/PW91k and PBE/revAPBEK, sDFT is in good agreement with KS-DFT, but in slightly better agreement with CCSD(T) reference data. Thus, there appears to be some error compensation between the NAXC and NAKE approximations that can be exploited.

The well-known problems associated with approximate KS-DFT in the description of dispersion interactions immediately raise the question whether sDFT can describe dispersion-dominated molecular complexes correctly. To address this question, Schlüns *et al.* [127] investigated the potential-energy curves obtained from sDFT with various combinations of NAXC and NAKE functionals. It turned out that the PW91 set of functionals, which are very popular in sDFT calculations, tend to overbind in many cases, while the combination of the BP86 NAXC functional with its “conjoint” counterpart LLP91 essentially reproduces the dispersion problems known in the context of KS-DFT for typical GGAs. This allows, in turn, to apply standard D3-type corrections [138, 139] to improve BP86/LLP91-sDFT calculations. By contrast, attempts to add empirical repulsive corrections to PW91/PW91k-sDFT calculations were less successful.

Similarly, one can investigate the accuracy of the structures of such non-covalently bound complexes obtained with sDFT geometry optimizations. Such studies were enabled by several new analytical gradient implementations for FDE/sDFT have appeared in the past

years, including a Slater-function-based code [140] in the AMSTERDAM DENSITY FUNCTIONAL FDE-module [141], and an implementation in the subsystem quantum chemistry program SERENITY [11, 137]. A benchmark study by Klahr *et al.* [137] of sDFT-optimized structures for the S22 and A24 test sets of intermolecular complexes (see Fig. 2a) found that popular combinations of NAXC/NAKE in FDE like LDA/Thomas-Fermi or PW91/PW91k describe the molecular structures reasonably well, but should be handled with extreme caution because of their inability to describe dispersion interactions. In contrast, for BP86/LLP91 with explicit D3(BJ) dispersion correction, the resulting structures showed very good agreement with the high-level reference data.

While conventional NAXC/NAKE approximations are not able to account for dispersion interactions and rely on D3-type corrections, by combining the non-local rVV10 xc functional [147] with the non-local LMGP kinetic-energy functional [61], the potential-energy curves of non-covalently bonded complexes can be reproduced accurately, including in cases in which the interaction is dominated by dispersion. With rVV10/LMGP, interaction energies across the S22-5 test set (which includes both equilibrium and displaced structures) are accurate within 1 kcal/mol. This impressive accuracy is preserved when combining the semilocal PBE functional with the GGA-level non-decomposable NAKE SMP, which mimics the nonlocal LMGP functional [61]. Note that in this case the NAXC does not account for dispersion interactions and, therefore, the excellent agreement observed in Ref. 61 must be due to error cancellation between the NAXC and NAKE functionals.

Another way of including the non-locality needed to describe long-range dispersion interactions within DFT is in terms of the fluctuation–dissipation theorem [148]. A corresponding subsystem DFT framework was established by Pavanello and co-workers [149] based on subsystem response functions. The resulting method has been denoted as FDE-vdW, as it aims at an improved description of van-der-Waals bonding situations. In fact,

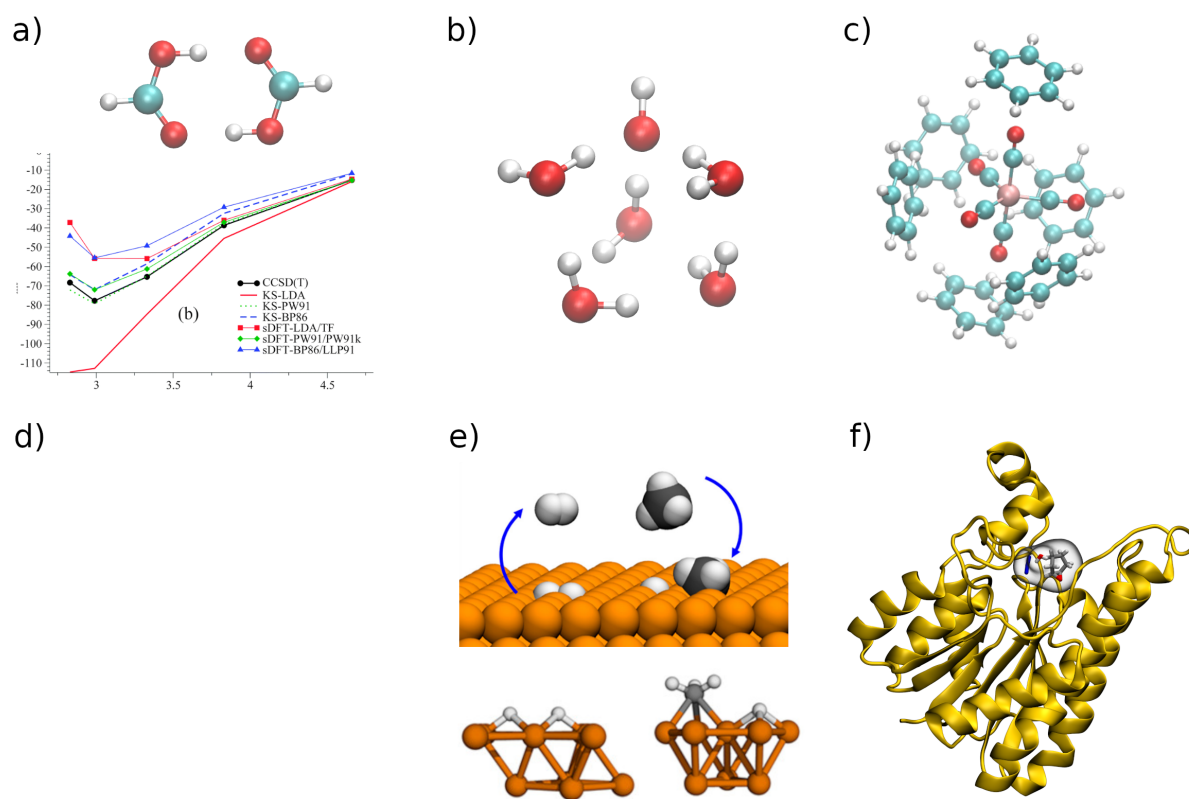


Figure 2: Different types of chemical systems to which sDFT/FDE are applied using various strategies. (a) Molecular dimers, such as the formic acid dimer; Adapted from Ref. 137 with permission from the PCCP Owner Societies. (b) Molecular clusters, such as the deprotonated water hexamer  $(\text{OH})(\text{H}_2\text{O})_5^-$  (see Ref. [142]). (c) Solvated molecules, such as  $\text{Fe}(\text{CO})_5$  solvated in benzene (see Ref. [143]). (d) Bulk interfaces, such as thiophene molecules physisorbed on a molybdenum sulfide monolayer deposited on  $\alpha$ -alumina (see Figure 3 in Ref. 144). (e) Adsorbed molecules, such as dihydrogen and methane on a copper surface; Adapted with permission from Ref. 145. Copyright 2020 American Chemical Society. (f) Proteins, such as halohydrin dehalogenase G (see Ref. 146).

the binding energies of such complexes are dramatically improved compared to sDFT employing semi-local exchange–correlation approximations. A further improvement, especially of potential-energy surfaces for such vdW systems, is possible by replacing the NAKE functionals in sDFT by the exact (Kohn–Sham) kinetic energy [150].

## 5.2 Molecular Clusters

While sDFT allows for the treatment of molecular clusters (see Fig. 2b) using the individual molecules as fragments, the accuracy of such an approach is limited by the accuracy of the NAKE approximation. A complementary subsystem approach is offered by the many-body expansion (for a recent review, see Ref. 151), which approximates the total energy of a molecular cluster as

$$E_{\text{tot}} = \sum_I E_I + \sum_{IJ} \Delta E_{IJ} + \sum_{IJK} \Delta E_{IJK} + \dots, \quad (23)$$

where  $E_I$  are the energies of the monomer fragments,  $\Delta E_{IJ}$  are the interaction energies of dimers,  $\Delta E_{IJK}$  are the interaction energies of trimer, and so on. This approach can be combined with sDFT/FDE in two different ways [152]. On the one hand, FDE can be used to include a frozen environment of the remaining fragments in the calculation of the monomer, dimer, trimer etc. energies. This accelerates the convergence of the many-body expansion (for a study in the context of FDE, see Ref. 153), but does not improve substantially compared to conventionally point-charge embedding.

On the other hand, sDFT can be used to provide a correction on top of a truncated many-body expansion. To this end, a many-body expansion of the total electron density is performed (see Fig. 3),

$$\rho_{\text{tot}}(\mathbf{r}) = \sum_I \rho_I(\mathbf{r}) + \sum_{IJ} \Delta \rho_{IJ}(\mathbf{r}) + \sum_{IJK} \Delta \rho_{IJK}(\mathbf{r}) + \dots. \quad (24)$$

As shown by our (CRJ’s) lab, this expansion can be inserted into the DFT total energy functional to arrive at a generalization of Eq. (3). Such a density-based many-body

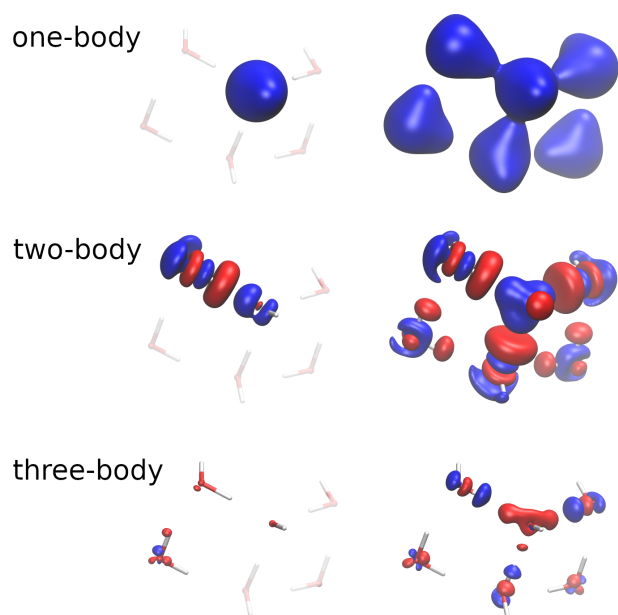


Figure 3: Illustration of the many-body expansion of the electron density for a deprotonated water hexamer,  $(\text{OH})(\text{H}_2\text{O})_5^-$  (see Ref. [142]). On the left, the contributions  $\rho_1(\mathbf{r})$ ,  $\rho_{12}(\mathbf{r})$ , and  $\rho_{123}(\mathbf{r})$  of a single monomer, dimer, and trimer, respectively, are visualized as isosurface plots (using isovalues of 0.05, 0.004, and 0.002, respectively). On the right, the one-body, two-body, and three-body contributions,  $\sum_I \rho_I(\mathbf{r})$ ,  $\sum_{IJ} \Delta\rho_{IJ}(\mathbf{r})$ , and  $\sum_{IJK} \Delta\rho_{IJK}(\mathbf{r})$ , respectively, to the total electron density of  $(\text{OH})(\text{H}_2\text{O})_5^-$  are shown (using the same isovalues).

expansion converges significantly faster than the corresponding energy-based many-body expansion, in particular if it is combined with frozen-density embedding for the fragment calculations. For water clusters [154] as well as ion–water clusters [142], it provides chemical accuracy (compared to the supermolecular calculation) already for a two-body expansion.

### 5.3 Solvated Molecules

The description of solvent effects on molecular properties has been one important application of FDE for many years (see, e.g., Refs. 6, 155–159). Typically, in such studies one performs molecular dynamics simulations using classical force fields or *ab initio* molecular dynamics to generate a sufficiently large number of structural snapshots. For each of these snapshots, one then uses FDE to calculate the molecular property of interest for the solvated molecule ( $\rho_I$ ) in the presence of the frozen solvent density ( $\rho_{II}$ ). This frozen density  $\rho_{II}$  is typically obtained as a sum of the electron densities of the isolated solvent molecules, possibly after partial relaxation in freeze–and–thaw cycles. The results for all snapshots are subsequently averaged. Recent examples of such studies can be found in Refs. 143, 160–164 (see Fig. 2c). It is worth noting that such a protocol can also be applied in combination with a treatment of the solute with wavefunction methods (WFT-in-DFT embedding, see Section 6.6) [160, 163] and that it can be combined with a (polarizable) force-field description of the outer solvent shells [164].

Wesolowski and coworkers investigated several aspects of such approaches for modeling solvent effects with FDE. First, different strategies for the choice of the solvent electron density were investigated. Humbert-Droz *et al.* [165] explored the sensitivity of calculated shifts in excitation energies with respect to the choice of the frozen density  $\rho_{II}$  for selected test cases of aromatic chromophores microsolvated by up to three water molecules. They found that a simple charge-weighted superposition of atomic densities leads to large varia-

tions in the excitation energies and strongly depends on the choice of atomic charges. The commonly used superposition of molecular electron densities (see, e.g., Refs. [155, 156]) turned out to be more stable and only showed a weak dependence on the basis set. Finally, the use of a frozen density from a single KS-DFT calculation for the solvent environment was also considered. Different strategies for including the polarization of the solvent molecules are compared in Ref. 166. An alternative to using a computed frozen density is explored in Ref. 167. Here, crystal structures of complexes of glycine dipeptide with a single solvent molecule were considered, and the frozen solvent density was extracted from the X-ray diffraction data, i.e., an “experimental” electron density was used as  $\rho_{II}$ .

Second, Wesolowski and coworkers explored replacing the averaging over several FDE calculations for each snapshot by performing a single FDE calculation using an averaged solvent electron density [168]. This way, the number of required quantum-chemical calculations of the molecular property of interest can be drastically reduced. It was shown that for the solvatochromic shift of the  $n \rightarrow \pi^*$  excitation of acetone in water, the effects of such an approximation are negligible. This observation was confirmed for the vertical excitation energies of protonated retinal Schiff bases in protein environments [169]. Such a strategy was further explored by analyzing the solvent fluctuations and by comparing different methods for the construction of the average solvent density [170].

In a similar spirit, instead of explicitly averaging over different solvent densities, more approximate schemes can be used to construct such an averaged solvent density. To this end, the reference site interaction model (RISM) [171, 172] was applied to obtain such an approximate average solvent density and apply it in combination with FDE [173] for the calculation of solvatochromic shifts in aminocoumarin C153 [174–176].

One of the basic properties relevant in the context of solvation are solvation free energies. Comparatively little effort has been spent on this aspect. In 2022, Bensberg *et al.* presented a strategy in which FDE is combined with a continuum solvation model for

the prediction of solvation free energies and their contributions to reaction energies and barriers in solution [177].

## 5.4 Bulk Systems and Interfaces

For the description of solvent effects, one focusses on a specific subsystems of interest in the condensed phase and applies FDE to include the effect of its surrounding environment. When treating condensed-phase systems themselves, such as liquids or molecular crystals, one can apply sDFT in order to exploit a partitioning into (molecular) subsystems, i.e., there is no specific subsystem of interest and all subsystems are treated on the same footing. This potentially offers an efficient, linear-scaling approach for the treatment of large, condensed-phase systems.

The sDFT approach has been implemented into program packages that use periodic boundary conditions. An early implementation in CP2K allowed for an arbitrary number of subsystems and was applied for molecular dynamics simulations of liquid water [178]. More recently, a new implementation of sDFT in CP2K was presented that makes use of linear scaling techniques and allows for the combination of sDFT with linear-scaling DFT [15]. It enabled impressive ground state and excited molecular dynamics simulations of systems as large as carbon nanotubes and the satellite tobacco mosaic virus in explicit water solvent.

Another implementation of sDFT with periodic boundary conditions based on the QuantumEspresso package was presented by Pavanello and coworkers [13, 14, 57]. It uses a plane-wave basis throughout and features full Brillouin zone sampling while allowing for an arbitrary number of subsystems. To exploit the locality of the subsystems, smaller overlapping boxes are used to restrict the size of the plane wave basis for each subsystem. This is combined with a sophisticated parallelization scheme for a distributed treatment

of the subsystems [13]. Applications include molecular dynamics simulations of liquid water [77], also addressing its optical spectrum [179], and supercritical CO<sub>2</sub> [180]. In addition, solid–solid and solid–liquid interfaces as well as surface–molecule interactions in complex condensed-phase systems [144, 181, 182] have been studied (see below).

Applications of sDFT for bulk systems critically depend on the accuracy of the employed NAKE approximation. For molecular dynamics simulations of liquid water, there has been some confusion whether conventional GGA functionals are applicable. While initially Hutter and coworkers found that the conventional GGA NAKes (in particular PW91k, LLP, and PBE) result in too weak hydrogen bonds and the absence of a structured second solvation shell [178], this finding could not be confirmed in later work. Pavanello demonstrated that GGA NAKes that perform well for the water dimer, such as revAPBEK, are able to reproduce the radial distribution function of liquid water (including a structured second solvation shell) accurately in sDFT molecular dynamics simulations [77]. The authors also claimed that sDFT might be superior to conventional KS-DFT as it avoids unphysical charge delocalization and thus partially cancels the inter-molecular self-interaction error of GGA xc-functionals. This was demonstrated for molecular dynamics simulations of a hydroxyl radical in aqueous solution. Recently, Pauletti *et al.* [183] combined sDFT with a  $\Delta$ -machine learning correction based on Behler’s neural network potentials [184], which was fitted to reproduce KS-DFT.

A specific advantage of sDFT is the accessibility of properties of the individual subsystems. This was exploited by Lubber to extract local dipole moments from KS-DFT-based molecular dynamics simulations, which enables the calculation of condensed-phase vibrational spectra [185] and provides an alternative to commonly used partitioning schemes, typically using maximally localized Wannier orbitals [186]. Later on, this idea was transferred to the context of real-time time-dependent DFT, where it can be used, e.g., for simulations of UV-Vis absorption spectra [187].

An extension of sDFT molecular dynamics to the nonadiabatic dynamics of excited states (treated within a  $\Delta$ SCF-DFT approach in combination with Tully's fewest-switches surface hopping) was presented by Mališ *et al.* [188]. It was applied to study a solvated diimine. Here, however, no full sDFT was performed, but only three subsystems were used, specifically the diimine, the water molecules in the first solvation shell, and the water molecules in the outer solvation shells.

To circumvent inaccuracies of approximate NAKEs for strongly interacting subsystems during molecular dynamics simulations in the liquid phase, Pavanello and co-workers presented a workflow in which subsystem boundaries are dynamically adjusted between different simulation steps [189], thus making sure that subsystems which interact too strongly are combined into one fragment. As a simple criterion for the interaction strength, the distances between subsystems are employed in that work.

Beyond liquids, sDFT can also be employed to describe complex solid–solid and solid–liquid interfaces in condensed-phase systems. As prototypical examples, Pavanello and coworkers [144] have applied their implementation of sDFT with periodic boundary conditions to a water bilayer on a platinum surface as well as to a complex system relevant for catalysis, consisting of a thiophene molecule physisorbed on a molybdenum sulfide monolayer, which is deposited on top of an  $\alpha$ -alumina support (see Fig. 2d). Here, each layer is treated as a separate subsystem. Efficiency gains compared to a conventional KS-DFT treatment can be obtained by adapting the  $k$ -point grid for each subsystem. For the molecular subsystem(s), considering only the  $\Gamma$ -point is sufficient, and also for the alumina layer the  $k$ -point grid can be reduced compared to the one used for the metallic layer. A similar strategy was applied for water and benzene on molybdenum sulfide surfaces [181, 182, 190]. To tackle even larger systems, sDFT can be further combined with orbital-free DFT for metallic subsystems, as was demonstrated for water and CO<sub>2</sub> on aluminium surfaces [191].

Also molecular implementations of sDFT can be extended towards to treatment of condensed-phase systems. Höfener and coworkers [192] have developed a scheme that imposes periodic boundary conditions in one dimension. To this end, an embedding potential is generated by periodically repeating the electron density of the active molecular subsystem, which is in turn used to embed this active subsystem into the environment of its own periodic images. This has been applied to calculate electron attachment and ionization as well as excitation energies in one-dimensional stacks of organic semiconductors [192,193].

3D quasi-periodic calculations have been achieved in terms of so-called *relax-copy-cycles* for molecular crystals [35]. During the relax step in these cycles, the orbitals of the molecules in an inner unit cell are determined, embedded in a guess electron density for the molecules in surrounding unit cells. Afterwards, the density in the surrounding unit cells is updated by copying the density of the innermost cell. This is repeated until the orbitals/densities of the molecules in the central unit cell do not change anymore. This strategy has been applied in Ref. 12 for spin-density calculations of clusters containing several thousand QM atoms (see also Section 6.5).

## 5.5 Impurities and adsorbed molecules

Subsystem DFT can be used to treat a localized impurity in a bulk system as a separate subsystem embedded in a periodic environment. Such a strategy has been employed extensively by Carter and coworkers to treat the adsorption of molecules on metal surfaces with WFT-in-DFT type calculations (see, e.g., Refs. 38,194), utilizing the DFET strategy as outlined in Section 4.3. Recent examples concern the electrochemical reduction of CO<sub>2</sub> on copper [195,196], and the electrochemical hydrogenation of CO on Cu(100) [197]. While complete active space self-consistent field (CASSCF) [198] or CASSCF augmented by second-order perturbation theory (CASPT2) [199] are commonly employed as wavefunction methods in such studies, embedded adaptive sampling configuration interaction

(ASCI) [200] has been considered if larger active spaces need to be treated. ASCI was used in a study on the H<sub>2</sub> desorption from and methane dissociation on copper surfaces, although it was found to be less successful than embedded CASPT2 for those examples [145] (see Fig. 2e).

A strategy for charged impurities has been developed by Tölle *et al.* [201]. Based on the density-embedding idea, a screening potential was defined in that work which, for the example of an ionized molecule as an impurity within a unit cell, replaces the electrostatic effect of the periodic impurity images by the potential of the neutral, non-ionized system. Treating such charged impurities is not straightforwardly possible with conventional methods under periodic boundary conditions. Recently, the ionization potential of water in water has been studied using this approach [202].

Finally, we note that as another example, a study on the X-ray photoabsorption spectrum of hydrogen chloride and chloride ions on ice surfaces or in water droplets based on FDE combined with relativistic core-valence separation equation-of-motion coupled cluster theory was presented by Gomes and co-workers [203].

## 5.6 Biomolecules

As the available approximations for the NAKE are typically not applicable for covalent bonds between subsystems, the treatment of biopolymers in general and proteins in particular (see Fig. 2f) with sDFT requires a strategy that circumvents this problem. To this end, a more general partitioning of the electron density that has been established in the molecular fractionation with conjugate caps (MFCC) method [204, 205],

$$\rho_{\text{tot}}(\mathbf{r}) = \sum_I \rho_I^{\text{frag}}(\mathbf{r}) - \sum_J \rho_J^{\text{cap}}(\mathbf{r}) \quad (25)$$

can be used. The protein is cut into fragments of one or more amino acids at the peptide bonds, and the severed bonds are capped with acetyl (ACE) groups and N-methylamide

(NME) capping groups, respectively, to preserve their chemical environment. In Eq. (25),  $\rho_I^{\text{frag}}(\mathbf{r})$  are the electron densities of the amino acid fragments and  $\rho_J^{\text{cap}}(\mathbf{r})$  are the electron densities of the ACE-NME cap molecules generated by joining neighboring capping groups.

Subsystem-DFT can then be reformulated using this generalized partitioning of the electron density [116]. To optimize the subsystem electron densities, the densities of the cap molecules are kept fixed and an additional constraint requiring the active subsystem density to equal the cap density at the ACE and NME caps is introduced. The latter is required to ensure the positivity of the total electron density. Accounting for this constraint requires an optimization of the potential in these cap regions similar to the one used in potential reconstruction schemes. This extension of sDFT to proteins has been termed three-partition frozen-density embedding (3-FDE).

First benchmark applications [116, 206, 207] demonstrated that by fully optimizing the electron densities of all subsystems in the presence of the protein environment 3-FDE provides electron densities and electrostatic potentials that are significantly more accurate than those calculated with the MFCC fragmentation scheme. The 3-FDE scheme has been used to obtain optimized electron densities for the the Fenna-Matthews-Olson protein, which where then used as environment in calculations of the embedded chromophores with FDEu-TDDFT [208]. This can be further combined with a continuum solvation model for the outer environment [209], for which an efficient local COSMO scheme has been developed [210].

With 3-FDE, the accuracy of the resulting electron densities is influenced by the choice of the amino acid fragments. In general, using larger fragments reduces the error introduced by the fragmentation. However, this error is strongly dependent on the protein structure. To determine near-optimal fragmentations for quantum-chemical fragmentation methods such as MFCC and 3-FDE, the use of graph partitioning algorithms has been explored

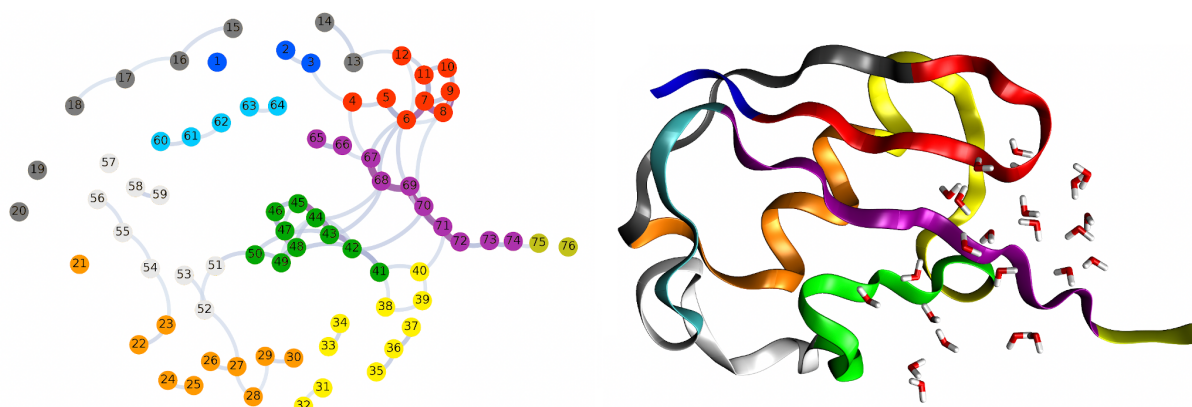


Figure 4: By mapping the expected error due to the fragmentation between two amino acids to a graph (left) it becomes possible to apply graph partitioning algorithms to identify optimal fragmentations that minimize this error (right). Here, such a scheme is illustrated for the protein ubiquitin. Adapted with permission from Ref. 146. Copyright 2021 American Chemical Society.

by our (CRJ's) lab [146,211] (see Fig. 4).

As an alternative approach to 3-FDE, one can of course restrict the biomolecular model environment to non-covalently bonded fragments. Following this strategy, spectral tuning effects resulting from specific interactions between chromophore and protein environment have been investigated for rhodopsin and various visual cone pigments in Ref. 212. While differential polarization/dynamic response effects of the environment have been explicitly neglected in that study, later work investigated these effects in terms of an embedded many-body expansion [153]. Vertical excitation energies for rhodopsin and three different visual cone pigments have also been calculated in Ref. 213 using NAKE-based CC2-in-DFT embedding. The models employed included part of the protein binding pockets, resulting in models with about 330 to 370 atoms in total. For enhanced efficiency, the authors presented an implementation of Laplace-transform scaled-opposite-spin CC2 version making use of the resolution-of-the-identity approximation.

# 6 Extensions of Subsystem Density-Functional Theory and Frozen-Density Embedding

## 6.1 Projection-based Embedding

### 6.1.1 Formal and algorithmic developments

A trend already briefly touched in our original article is to entirely avoid the need for a NAKE functional and the corresponding NAKP potential by enforcing the mutual orthogonality of the subsystems. One flavor of such an approach was introduced in a work by Khait and Hoffmann [103], where explicit Lagrangian multipliers were introduced in the variational optimization procedure to ensure mutual orthogonality of the subsystem orbitals. While it was erroneously combined with a NAKE approximation in this original article, the use of additional NAKE components was avoided in later work [104]. Subsequent work demonstrated that this method makes it possible to describe bond-dissociation processes [214]. In parallel, Manby, Miller and co-workers had proposed an embedding scheme in which external orthogonality was introduced in terms of a level-shift operator, which shifted the occupied orbitals of the environment systems to very high energies and hence made them effectively orthogonal to the occupied orbitals of the active subsystem [215]. While the external orthogonality represents a fundamental difference to the original formulation of sDFT and FDE, all other ingredients in energy and potential expressions (apart from a perturbative correction for finite level-shift parameters [215]) are identical in this level-shift embedding. Hence, the latter can, from the sDFT perspective, be regarded as an FDE variant in which the NAKP has pragmatically been replaced by a projection operator, so that the non-additive kinetic energy simply vanishes. As might seem obvious, the two schemes are closely related to each other. An independent implementation of the level-shift approach was presented by Chulhai and Jensen in 2015 [105]

and applied to subsystems connected by aromatic bonds. A third variant of PbE was introduced by Kállay and co-workers in 2016 [216], which explicitly related to the partitioning of Slater determinant wavefunctions in the context of Hartree–Fock calculations developed by Huzinaga and Cantu [217]. The projection operator derived in that work is essentially identical to that by Khait and Hoffmann, and only differs in the way that Hermiticity of the resulting Fock operator is ensured.

For all three PbE variants discussed above, the subsystem orbitals of a subsystem  $A$  interacting with another subsystem  $B$  are obtained by solving,

$$(\hat{f} + \hat{O})\phi_{i_A} = \epsilon_{i_A}\phi_{i_A} \quad (26)$$

where  $\hat{f}$  is the supermolecular Kohn–Sham–Fock operator, and the three common choices for the operator  $\hat{O}$  are either the level-shift operator as employed by Manby, Miller and co-workers [215],

$$\hat{O}_1 = \lim_{\mu \rightarrow \infty} \mu \hat{P}^B, \quad (27)$$

where the scaling factor  $\mu$  is in practice chosen large but finite, or the Huzinaga operator [217],

$$\hat{O}_2 = -[\hat{f}, \hat{P}^B]_+, \quad (28)$$

(where the index  $+$  indicates the anticommutator; note the typo in Ref. 218), or the operator employed by Hoffmann,

$$\hat{O}_3 = \hat{P}^B \hat{f} \hat{P}^B - [\hat{f}, \hat{P}^B]_+, \quad (29)$$

with the projector onto the environment orbitals (orbitals of the environment subsystem  $B$ )

$$\hat{P}^B = \sum_{j \in B} |\phi_{j_B}\rangle \langle \phi_{j_B}| \quad (30)$$

As a slight digression, we note that the approach by Huzinaga and Cantu had been introduced pragmatically in the QM/QM/MM model by Olsen *et al.* [219,220], (which shares several elements with FDE concerning the QM/QM part) to mimic Pauli repulsion effects between the core and inner QM regions. In practical terms, an important aspect of this so-called polarizable density embedding (PDE) is that the computationally rather demanding freeze-and-thaw iterations for mutual polarization of the subsystems is replaced by a polarizable MM treatment in terms of induced dipoles. A similar strategy was later on also used by Jensen and co-workers [221] by combining a polarizable MM strategy with FDE and the level-shift operator technique to ensure external orthogonality.

As an alternative to the projection schemes mentioned above, Hammes-Schiffer and co-workers enforced EO by projecting the active orbitals of the environment out of the basis set of the active system [222], which followed an approach by Hunt *et al.* [223]. Closely related to PbE is also the multilevel DFT approach by Cappelli, Koch, and coworkers [224,225], which effectively also works with a partitioning into orthogonal active and embedding orbital spaces [226]. But instead of explicit projection operators, their scheme uses an exponential parametrization of the subsystem density matrices to ensure the orthogonality of the subsystems during energy optimization.

Strictly speaking, PbE methods do not primarily partition the electron density, but are based on a separation of orbitals into sets for different subsystems. In the original work by Manby, Miller and co-workers [215], this was applied in a top-down fashion. In this case, the calculation starts with an SCF calculation on the supersystem, followed by an orbital localization. Then, the orbitals for the active system may be defined in a certain way (see below), while all orbitals not selected for the active system constitute the environment system and are incorporated into the projection operator. Since a supermolecular SCF calculation is needed, this approach cannot offer efficiency gains compared to the total-system calculation. However, such PbE calculations often form the starting point for

more advanced wavefunction-in-DFT embedding calculations with covalent bonds between the wavefunction and the DFT region. Since the active region usually contains much fewer electrons than the total system, large computational savings might be expected. A difficulty here lies in the fact that the procedure is only exact if the entire basis of the environment is included in the calculation of the active system. Because of this, the total number of orbitals (occupied and virtual) in the subsystem calculation on the active system is the same as in the supersystem calculation. However, the number of occupied orbitals is reduced by the number of occupied orbitals in the environment system, whereas the number of virtual orbitals is increased by the same amount, which can even lead to a formal *increase* in computational cost. Hence, several strategies have been proposed to truncate the basis used in these PbE calculations. From an efficiency point of view, it seems advantageous to restrict the basis to functions on the active system only. However, this usually leads to difficulties in constructing the projection operator which has to ensure the orthogonality to the environment orbitals.

Barnes *et al.* proposed a truncation scheme in which “active” and “border” atoms are defined [227]. Only basis functions centered at those atoms are employed in the calculation of the active system, including the construction of the projection operator for embedding. Only orbitals mainly centered on the border atoms were included in the projection operator, whereas molecular orbitals located on more distant atoms were treated in terms of an approximate, non-additive kinetic potential contribution. Bennie *et al.* later introduced a basis-set truncation scheme based on a Mulliken population analysis for the atoms of the active system [228]. In Refs. 229, 230 these two strategies for top-down PbE were combined and tested for all three variants of PbE (Level-Shift, Hoffmann-type projection, and Huzinaga equation); the Huzinaga-operator strategy turned out to behave most favorably with respect to the basis-set truncation. In addition, an automatic basis-set *extension* was proposed for bottom-up PbE calculations in that work, in which the reference basis set is just the monomolecular basis set of the active system. Another strategy in terms

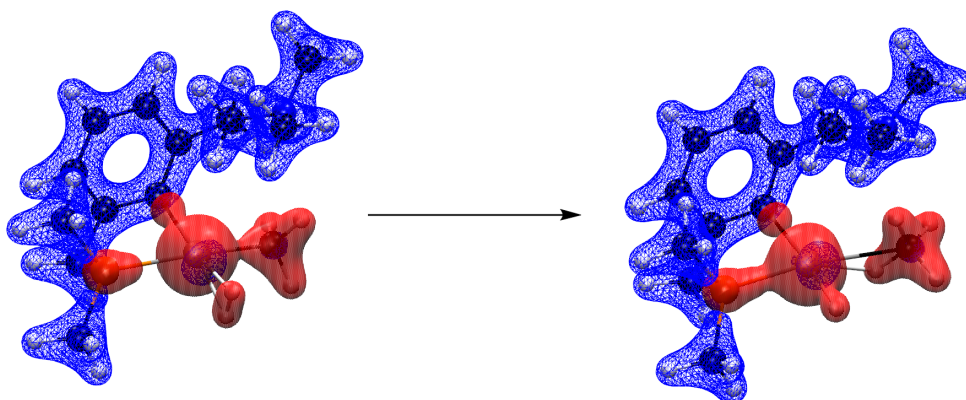


Figure 5: Illustration of the orbital/density partitioning in the direct-orbital-selection (DOS) algorithm from Ref. 232: The isosurfaces visualize the frozen environment (blue) and active (red) parts of the electron density, based on the corresponding orbitals selected determined via DOS. Note, for instance, that core orbitals at the metal center form a frozen part inside the active valence electron density in this case. The isosurfaces have been obtained from a HF-in-BLYP/def2-TZVP calculation using a DOS selection threshold of 0.05 for reaction no. 30 from the MOBH 35 test set [233] (coordinates taken from Ref. 234).

of a dual-basis approach for embedding calculations was proposed by the Kállay group in 2018 [231].

In most of these studies, the definition of the active system was based on a set of manually selected active atoms in combination with a Mulliken population analysis or based on the Boughton–Pulay algorithm [216]. Alternatively, Claudino and Mayhall developed an orbital-selection strategy based on a singular value decomposition [235,236]. A different strategy was proposed in Ref. 232 (see Fig. 5). There, a combined criterion of orbital kinetic energies and orbitalwise atomic charges was employed to directly determine active orbitals in PbE calculations as those orbitals that significantly change during a reaction. This can be regarded as a more direct active-system definition in the context of PbE, since the projector requires a partitioning of the occupied orbital space, rather than a partitioning on the basis of “atoms” or “densities”. This was later refined using an orbital alignment criterion [237], transferred to WF-in-DFT embedding [37], and to multi-level

coupled-cluster hybrid methods [238]. The direct orbital selection from Ref. 232 also automatically solves the problem of selecting subsystems in an “even-handed” manner, which was brought up in Ref. 239.

In another line of development, the Goodpaster group followed the strategy of restricting the basis set for the calculation of the embedded system to a monomer basis only [240]. This “absolute localization” makes use of the Huzinaga-type projection operator, for which the effect of using a heavily truncated basis is much less severe than for the level-shift projection operator. Another crucial ingredient is the correction of the WF-in-DFT energy thus obtained by the difference between a KS-DFT supersystem energy and the corresponding DFT-in-DFT embedding energy based on absolute localization. The latter correction is intended to mitigate effects at the boundary region between subsystems, especially when cutting through covalent bonds. The approach has been combined with various wavefunction schemes such as CCSD(T), CASPT(2) [241], and a variant of full configuration interaction quantum Monte Carlo [242]. Recently, it has also been combined with wavefunction methods for open-shell systems such as unrestricted and restricted open-shell CCSD(T) as well as with CASPT2. It could efficiently and successfully be applied for calculations of radical reactions and spin-transition energies [243]. We note in passing that the block-localized density functional theory developed by Gao and co-workers [244], based on the corresponding block-localized wave function method by Mo and Peyerimhoff [245], shares the elements of (i) a restriction to a monomer (“subgroup”) basis for each subsystem, and (ii) a employing a projection operator in the calculation of the block-localized orbitals, albeit of Hoffmann-type as presented in Eq. (29), with this absolutely-localized PbE.

An analysis of the remaining error sources in projection-based WF-in-DFT embedding showed that the main problem is the non-additive exchange–correlation energy [246], for which an MP2-type correction was proposed. In the context of transition-metal chem-

istry, this topic has been picked up in our (JN's) lab [37]. It was shown that WF-in-DFT embedding can actually lead to worse results than DFT-in-DFT embedding for the same system, since the “improved” wavefunction description of the active system destroys the error cancellation between errors in the active-system's energy and the interaction energy. The problem can be mitigated by choosing a more sophisticated NAXC functional, e.g., a double hybrid, while using a more economic functional for the XC energy of the environment, as was recently confirmed in a benchmark study on transition-metal chemistry [234]. Alternatively, a larger active system (i.e., more active orbitals) may have to be chosen. A recent addition to the arsenal of projection-based wavefunction-in-DFT methods is the DMRG-in-DFT combination presented by Beran *et al.* [247]. One important ingredient for the applicability of PbE WF-in-DFT embedding is the ability to optimize structures consistently with the energy calculations. The corresponding theoretical framework has been worked out by Lee *et al.* in 2019 [248] and implemented in MOLPRO. That work also contains a first set of examples for which structures have been optimized, including applications to a transition-metal complex.

For applications of PbE on open-shell systems, approximate density-functional theory can lead to substantial errors in the DFT region due to the effects of the self-interaction error (SIE). Pennifold *et al.* showed that in such cases WF-in-HF calculations can actually produce more accurate results than the corresponding WF-in-DFT calculations, since the Hartree–Fock method avoids the overdelocalization/SIE problems of approximate DFT [249]. Chulhai and Goodpaster presented a version of PbE-type WF-in-DFT embedding for periodic systems in 2018 [250].

Projection-based embedding is recently being pushed forward in emerging new fields of quantum chemistry. Pavošević and Rubio developed an PbE-type embedding in the context of polaritonic chemistry, leading to quantum-electrodynamics coupled cluster (QED-CC) in QED-SCF embedding [251]. Excellent agreement of such QED-CC-in-QED-SCF

results with the data of full QED-CC calculations was reported for reactions like a methyl transfer in an optical cavity.

### 6.1.2 Applications of PbE

Stella *et al.* have studied the adsorption of cobalt on small aromatic model systems for graphene. Their comparison of various density-functional approximations, projection-based coupled-cluster-in-DFT embedding, and full coupled-cluster calculations underline that the dependence on the choice of approximate XC functionals is considerably reduced in the projector-embedding approaches, which are also more consistent with experimental data [252].

Huo *et al.* investigated the suitability of pyridyl-substituted cobalt catalysts for decoupling the energetics of metal site reduction and metal hydride formation in potential inorganic hydrogen evolution catalysts [253] by means of projection-based CCSD(T)-in-DFT embedding. As also in this case the decisive reaction step investigated is a proton transfer, so that the PbE calculations could be carried out very efficiently and with high accuracy, leading to the identification of promising catalyst candidates. The role of second-sphere amines as proton donors in cobalt catalysts for CO<sub>2</sub> reduction was theoretically investigated in work by Miller, Marinescu, and co-workers [254]. Standard DFT analysis were augmented and backed up by PbE calculations, where in particular CCSD-in-DFT and, in view of rather large T1 diagnostics, MR-CISD-in-DFT embedding was employed. The observed decrease in activation barriers ranged up to 7.9 kcal/mol, but left qualitative conclusions unchanged.

The first application of PbE-type CC-in-DFT embedding with an outer MM layer to an enzymatic reaction was presented by Bennie *et al.* in 2016 [255]. That worked showed in particular the high accuracy and low dependence on the XC functional for the DFT

part in calculations. The reaction in question, a proton abstraction from acetyl-coenzyme A, is a prototypical example for a reaction well suited for multilevel schemes, as the reaction and the associated changes in the electronic (and geometric) structure are highly localized. Subsequently, Zhang *et al.* investigated the formation of fluorocitrate in an enzymatic reaction responsible for the action of fluoroacetate as a pesticide. The energy profile for this enantioselective reaction was calculated with projection-based CCSD(T)-in-DFT/MM embedding, again highlighting the possibility to efficiently generate CCSD(T)-quality reaction energetics with only small dependence on the choice of the XC energy functional [256].

Miller and co-workers employed projection-based embedding to predict vertical ionization energies of ethylene carbonate and dimethyl carbonate (DMC) in condensed phase, including mixtures of the two compounds [257]. Especially for DMC it was found that simple dielectric continuum models do not accurately reproduce the reorganization energy obtained from PbE calculations combined with configurational sampling of classical MD snapshots.

The electronic absorption spectrum of a ruthenium nitrosyl complex have been studied by means of PbE-CASSCF-in-DFT calculations by Galembeck and co-workers [258]. The calculations led to good agreement with the experimental spectrum in particular at short wavelengths. It could be shown that it is essential to include spin-orbit coupling effects, since several spin-forbidden transitions occur.

## 6.2 Extensions to Excited States

Methods to calculate energies of excited states or excitation energies, respectively, have already been discussed in detail in our original review [5]. As the two principle ways to calculate excitation energies, difference-based methods of  $\Delta$ SCF-DFT type as well as

linear-response time-dependent density functional theory transferred to the subsystem DFT context have been mentioned in that context, even though the former approach was only briefly touched. In the mean time, both classes of methods have been considerably further developed, as will be explained in the following. We would like to note that the topic of excited states will be picked up again in the context of WF-in-DFT-embedding in Section 6.6.2.

### 6.2.1 Energy-difference-based methods

Conceptually the most straightforward way to determine excitation energies of quantum mechanical systems is calculating the electronic energy for different electronic states [typically the ground state (GS) and an excited state (ES)], and then computing their difference,

$$\Delta E = E_{\text{ES}} - E_{\text{GS}}. \quad (31)$$

A technically rather simple approach of this type is the  $\Delta$ SCF method, in which  $E_{\text{ES}}$  is obtained by converging a self-consistent field calculation not to the ground state, but rather to an excited state. In the context of FDE/sDFT, this strategy has been in use for a long time already, even though with different sophistication and approximations. In 2006, Leopoldini *et al.* investigated the spin-state dependence of possible reaction pathways in models for a nitrate reductase via separate FDE-type SCF calculations for singlet and triplet states [259]. This is arguably the most straightforward type of application of  $\Delta$ SCF, since no issues related to a possible collapse to the ground state occur because of different spin symmetry of the states involved. A study on the calculation of singlet–singlet excitation energies of a molecule in an environment that made use of FDE- $\Delta$ SCF approaches was performed in a collaboration of our (JN’s) lab with the Filippi group [260, 261]. There, however, the  $\Delta$ SCF approach was only used to polarize the environment densities in a state-specific manner for subsequent use in WF-in-DFT calcu-

lations. In Ref. 262, FDE- $\Delta$ SCF was employed to describe a local  $\pi \rightarrow \pi^*$  excitation in an ethene monomer in the presence of a second ethene molecule. The actual goal in that study was to employ the resulting orbitals for the definition of a diabatic state and the subsequent calculation of electronic coupling-matrix elements to a charge-transfer state (see also Sec. 6.3). One main advantage of  $\Delta$ SCF-DFT over the corresponding linear-response TDDFT approach is the easy availability of analytical gradients, which allows a straightforward application to excited-state dynamics. This route was followed in recent work by the Lubber group to facilitate efficient non-adiabatic molecular dynamics of a diimide system in water [188].

In this context, a conceptually very important issue arises, which was formally discussed already by Khait and Hoffmann in 2010 [263] and put into practice in Ref. 260: If the densities  $\rho_I$  and  $\rho_{II}$  of the active system and environment, respectively, are mutually relaxed in a self-consistent manner, the resulting embedding potentials (for the active system in particular) will be different for different electronic states. We note in passing that this effect also appears in other types of embedding schemes, like polarizable QM/MM, where the polarization of the environment is state-dependent if evaluated self-consistently. Explicitly considering this state-dependence has the advantage that differential polarization effects can be captured, which is particularly important if density rearrangements between different electronic states are large. An example is the  $\pi \rightarrow \pi^*$  excitation of methylenecyclopropane microsolvated by water, which served as an example in Ref. 261. Here, the dipole-moment change between the ground and the excited state amounts to about 3–4 Debye, depending on the number of water molecules considered. In such cases, the  $\rho_{II}$ -dependent differential electrostatic embedding effect can be expected to dominate the changes in the embedding potential, and the state-specific embedding potentials often show better results than state-universal approximations. However, subsequent work on the green fluorescent protein [264] indicated that state-specific embedding potentials alone are not suited to capture all relevant effects. Based on a polarizable classical embed-

ding model, it was shown that a linear-response formulation of the interaction between chromophore and environment can lead to more accurate results.

Another important consequence of using state-specific embedding potentials is that the resulting ground- and excited-state wavefunction are no longer orthogonal [260]. This even holds if the environment density is assumed to be state-independent, since the embedding potential depends also on the active system's density, which of course differs between different electronic states. If the embedding potential is constructed based on a common reference density for the active system for ground- and excited states as a further approximation, a state-universal embedding potential is obtained [260]. This is essentially the same as the linearization approximation suggested in Ref. 265, which also contains a formal analysis of embedding potentials in the context of FDET, and a summary of advantages and disadvantages of different approximations.

### 6.2.2 Subsystem TDDFT

The theoretical background of subsystem TDDFT (sTDDFT) has been reviewed both in our original article [5] and in a perspective article focussing on this topic [266,267], which also discusses recent applications of sTDDFT. Here, we briefly repeat some of the basic ideas and working equations with a special focus on recent developments, mainly following the presentation in Refs. 218,268. For the sake of brevity, we will omit spin labels in the following; the full formalism explicitly considering spin labels is given in Ref. 268, and an earlier derivation of the unrestricted formalism (neglecting environmental response, however) can be found in Ref. 269.

Subsystem TDDFT is based on the idea that not only the electron density, but also the response in the density (for a certain frequency  $\omega$ ) to an external perturbation can be

separated into subsystem contributions, i.e.,

$$\delta\rho(\mathbf{r}, \omega) = \sum_I \delta\rho_I(\mathbf{r}, \omega).$$

Subsystem contributions to the density response can be expanded in terms of the perturbed density matrix elements  $\delta P_{(ia)_I}$  and  $\delta P_{(ai)_I}$ , where  $i, j, \dots$  and  $a, b, \dots$  refer to occupied and virtual orbitals, respectively,

$$\delta\rho_I(\mathbf{r}, \omega) = \sum_{i_I, a_I} (\delta P_{(ia)_I} + \delta P_{(ai)_I}) \phi_{i_I}(\mathbf{r}) \phi_{a_I}(\mathbf{r}).$$

Similarly to conventional TDDFT, the resulting response equations for the case of resonance with the incident frequency  $\omega$  can be cast into the non-Hermitian eigenvalue problem,

$$\left[ \begin{pmatrix} \mathbf{A} & \mathbf{B} \\ \mathbf{B} & \mathbf{A} \end{pmatrix} - \omega \begin{pmatrix} -\mathbf{1} & \mathbf{0} \\ \mathbf{0} & \mathbf{1} \end{pmatrix} \right] \begin{pmatrix} \mathbf{X} \\ \mathbf{Y} \end{pmatrix} = \begin{pmatrix} \mathbf{0} \\ \mathbf{0} \end{pmatrix} \quad (32)$$

where the matrices  $\mathbf{A}$  and  $\mathbf{B}$  as well as the solution vectors  $\mathbf{X}$  and  $\mathbf{Y}$  show a subsystem structure (subsystems indicated through indices  $I, J$ ),

$$A_{(ia)_I, (jb)_J} = \delta_{IJ} \delta_{ij} \delta_{ab} (\epsilon_a^I - \epsilon_i^I) + K_{(ia)_I, (jb)_J}, \quad (33)$$

$$B_{(ia)_I, (jb)_J} = K_{(ia)_I, (bj)_J}, \quad (34)$$

$$X_{(ia)_I} = \delta P_{(ia)_I}, \quad (35)$$

$$Y_{(ia)_I} = \delta P_{(ai)_I}, \quad (36)$$

with coupling-matrix elements (in Mulliken notation)  $K_{(ia)_I, (jb)_J}$ ,

$$K_{(ia)_I, (jb)_J} = (i^I a^I | j^J b^J) + (i^I a^I | f_{\text{xc}}(\mathbf{r}, \mathbf{r}') | j^J b^J) + (i^I a^I | f_{\text{kin}}(\mathbf{r}, \mathbf{r}') | j^J b^J) \quad (37)$$

$$- \delta_{IJ} (i^I a^I | f_{\text{kin}}^I(\mathbf{r}, \mathbf{r}') | j^J b^J) - c_x (i^I j^J | a^I b^J). \quad (38)$$

Here,  $f_{\text{xc}}$  and  $f_{\text{kin}}$  contain second functional derivatives of the exchange–correlation and kinetic-energy functionals, respectively, and  $f_{\text{kin}}^I$  is an intra-subsystem kinetic-energy kernel.

A number of approximations can be introduced at this point. Just as in standard TDDFT, the Tamm–Dancoff approximation (TDA) can be applied by setting the  $\mathbf{B}$  matrix to zero in Eq. (32), as has been introduced in Ref. 270. More importantly, a hierarchy of approximations can be devised based on the subsystem structure of the matrices above, both in the full sTDDFT problem and in its TDA version. As a first step, the “uncoupled” (FDEu-TDDFT) approximation to the response problem above is obtained by considering only the subsystem-diagonal blocks (with elements  $A_{(ia)_I,(jb)_I}$  and  $B_{(ia)_I,(jb)_I}$ ) for a particular subsystem  $I$ , but neglecting the response of and response coupling to all other subsystems. Second, an approximate “coupled” (FDEc-TDDFT) solution can be obtained by generating a few of the lowest-lying FDEu-TDDFT excitations for several subsystems, and solving the subsystem TDDFT problem in the basis of those subsystem-localized excitations. This can be considered as a subspace projection of the full response problem in Eq. (32) into a predefined space of subsystem-localized excitations, and is often useful when dealing with problems related to excitonic couplings in chromophore aggregates. And third, if this treatment needs further refinement, the solution vectors obtained in the second step can be employed as guess vectors for a full solution of Eq. (32) based on iterative subspace methods. Full details of this hierarchy are presented in Ref. 268.

Many applications of approximate sTDDFT have to deal with three important practical limitations: (i) the neglect of environmental response contributions and couplings between active-system and environment response; (ii) the use of an approximate NAKE functional, which has consequences both in terms of the associated NAKP affecting orbitals and orbital energies, and in terms of the (non-additive) kinetic kernel contributions entering the coupling matrix; and (iii) the use of monomer basis sets, which are usually chosen for reasons of efficiency. While issue (i) can in principle be addressed in terms of the hierarchy discussed above, the practical success may be intertwined with the strategies to tackle the other two problems: If a monomer basis set is employed, no inter-subsystem charge-transfer excitations can be described by construction, since the orbital product

space is simply not flexible enough to allow “outgoing” charge-transfer excitations. But a supermolecular basis set is usually also not suitable, since the virtual orbitals localized in the environment will, in general, have an incorrect structure due to the deficiencies of the NAKPs (see the discussion below).

Concerning the problems related to approximate NAKE functionals, the two solution strategies of either using reconstructed embedding potentials or switching to a projection-based embedding formalism as an alternative have both been transferred to the subsystem TDDFT context as well. As already mentioned in Section 4.3, the work in Ref. 107 employed reconstructed embedding potentials, which considerably improved the accuracy of excitation energies for local excitations, even though no corrections to the NAKE–NAXC kernel had been considered. One particular problem in connection with approximate NAKPs is the possible electron leaking (or electron spill-out) if diffuse monomer or even supermolecular basis sets are employed. In connection with excited states, especially the structure of unoccupied orbitals can suffer dramatically from that problem [64]. In a pragmatic approach avoiding the need for reconstructing potentials, Treß *et al.* used all-electron pseudopotentials for atoms in the environment in addition to the standard approximate embedding potentials to mimic the effect of repulsive potential contributions [271]. A related approach had been proposed by Hättig and co-workers within the QM/MM-context before [272]. For their test set comprising 11 systems, including solvated molecules, host–guest systems, and complexes of (small) organic molecules, the mean absolute deviation for excitation energies could be considerably reduced in this way.

As an alternative, projection techniques have been pushed forward. These approaches make use of orbitals and orbital energies obtained from the corresponding ground-state PbE problem shown in Eq. (26). In that case, there are no kinetic-energy-related kernel contributions in the coupling matrix. Instead the kernel contributions arising from the

projection operator are given by (assuming two subsystems denoted as  $A$  and  $B$ ) [268,273],

$$\begin{aligned}K_{(ia)_A,(jb)_B}^{\hat{O}_1} &= \mu S_{ij}^{AB} S_{ba}^{BA} \\K_{(ia)_A,(jb)_B}^{\hat{O}_2,\hat{O}_3} &= -F_{ij}^{AB} S_{ba}^{BA}\end{aligned}$$

for the  $\mathbf{A}$  matrix and

$$\begin{aligned}K_{(ia)_A,(bj)_B}^{\hat{O}_1} &= \mu S_{ib}^{AB} S_{ja}^{BA} \\K_{(ia)_A,(bj)_B}^{\hat{O}_2,\hat{O}_3} &= -F_{ib}^{AB} S_{ja}^{BA} - S_{ib}^{AB} F_{ja}^{BA}\end{aligned}$$

for the  $\mathbf{B}$  matrix.

In 2016, Chulhai and Jensen made a first attempt to transfer the concept of external orthogonality to subsystem TDDFT [274]. In their work, however, a symmetric eigenvalue problem was derived by implicitly assuming that the PbE kernel contributions are identical for the  $\mathbf{A}$  and  $\mathbf{B}$  matrices, which leads to deviations from corresponding Kohn–Sham supersystem results. The “exact” version of subsystem TDDFT was derived for all three different projection operators considered above in work from our (JN’s) lab in 2018 [268,273]. It could be demonstrated that this exact sTDDFT (when using the full supermolecular basis in each subsystem calculation and considering the full space of orbital transitions of all subsystems) is equivalent to a supermolecular TDDFT formulated in localized molecular orbitals (LMO). Hence, all three major problems mentioned above can be solved by this approach. Another benefit of using PbE is that XC approximations incorporating exact exchange contributions can be easily used, which is problematic if the subsystem orbitals are not externally orthogonal. This is important for TDDFT-type calculations, for which hybrid functionals and in particular range-separated hybrids are very popular.

The ground-state projection in PbE ensures that every subsystem consists of a set of occupied orbitals localized in the region associated with that subsystem, and, in addition, of the entire (supersystem) set of virtual orbitals. This has the effect that even outgo-

ing charge-transfer excitations for each subsystem can be described. Because of this, the method is also suited to described couplings between local excitations and charge-transfer excitations, for which it gives results in line with methods like the fragment excitation difference (FED)-fragment charge difference (FCD) diabaticization procedure [275]. Since this exact sTDDFT provides a robust reference for the quantification of environment effects, it was also applied in a proof-of-principle study to describe environmental response contributions also known as off-resonance excitonic couplings [276]. In that work, also a new type of virtual-orbital localization procedure was employed, based on earlier work by Claudino and Mayhall [235], in order to separate the effect of local and inter-subsystem charge-transfer excitations.

The exact sTDDFT strategy to fully cover the environmental response is, however, very costly. To mitigate the computational burden, also a cumulative evaluation of response effects of individual environment subsystems was successfully introduced. But even this turned out to be too costly in large production-scale calculations addressing, for instance, chromophores in protein-model environments. For this class of problems, a combination of FDE-based TDDFT and an embedded many-body approach was successfully introduced [153]. If the problem at hand involves resonant excitonic couplings between a large number of chromophores, further simplifications may be made. This involves the combination of subsystem TDDFT with Grimme's simplified TDDFT and/or the connection to more pragmatic exciton coupling approaches based on approximate Coulomb couplings. A description of such an approach, which also points out the connection between the simplified TDDFT approach (within the Tamm–Dancoff approximation) and transition-charge-based Coulomb couplings is provided in Ref. 277. We note that the above-mentioned equivalence to an LMO-based TDDFT scheme is highlighted by comparison to an alternative recent development for characterizing excited states in terms of an LMO-TDDFT approach [278].

Bennie *et al.* have combined PbE with equation-of-motion CCSD for the calculation of local excitation energies of solvated systems [279]. This enabled excitation-energy calculations of comparatively large solvated cluster like acrolein in up to 37 water molecules. It has to be noted that such calculations necessarily include the virtual orbitals formally located in the environment region (unless truncation schemes are applied), which helps to describe certain types of environment response effects (outgoing CT), but at the same time adds to the computational burden. For smaller system sizes, where full EOM-CCSD calculations could still be conducted, the error of the PbE-EOM-CCSD calculations was within 0.01 eV. Another detailed analysis of PbE-EOM-CCSD results including excitation energies, electronic resonances, but also ionization and electron attachment processes, has been presented by Parravicini and Jagau [280].

In the context of absolutely localized PbE, the Goodpaster group has presented an extension for excited states [281]. A state-averaged polarization of the active system was tested in that work in addition to the standard, ground-state polarization applied to the active subsystem before the linear-response (or EOM, in case of coupled cluster calculations) step. While this state-averaged polarization did not systematically improve the results for the examples studied in that work, an alternative correction term to the excitation energy, calculated as the difference between the supersystem TDDFT and the FDE-TDDFT excitation energy of the active system, turned out to be more promising. This, however, requires a mapping of the excitations from the active system to the supersystem.

Besides the developments addressing the three important issues discussed above, there has also been progress concerning new features in relation to sTDDFT. For a discussion of approaches incorporating linear-response wavefunction methods, we refer to Section 6.6.2. Efforts have been made towards a characterization of excited-state potential-energy landscapes of embedded chromophores. There has been a first implementation of analytical gradients for FDE-TDDFT excitation energies published in 2016 [282], followed by

several articles by Höfener and co-workers, including work on gradients for excitation energies from embedded linear-response CC2 and ADC2 (in addition to DFT-in-DFT embedding) [283–286].

Non-adiabatic dynamics using subsystem TDDFT by means of Ehrenfest MD have been presented by VandeVondele and co-workers [15] using examples such as the absorption spectrum of a typical dye molecule used in dye-sensitized solar cells, solvated in acetonitrile, or the dynamics of an electron injected into a boron–nitride nanotube.

Another branch of development concerns the real-time versions of subsystem TDDFT [25] and time-dependent potential-functional embedding theory [287]. The Pavanello group has demonstrated how to investigate system–bath couplings in the framework of real-time subsystem TDDFT, considering one of the subsystems as an open quantum system and another one as a bath [288]. Based on a decomposition of the linear-response functions, Markovian and non-Markovian effects can be distinguished in this formalism. An implementation employing localized basis functions was presented by De Santis *et al.* [289], making use of the PyADF scripting framework [290] for connecting the PSI4 code [291] (via the Psi4Numpy API [292]) with the AMSTERDAM DENSITY FUNCTIONAL (ADF) program [293, 294].

### 6.3 FDE as a Diabatization Tool

In our original article [5], we have outlined that typical deficiencies of FDE calculations can, in some cases, actually be turned into an advantage. This is the case since standard approximations for the NAKP are often too repulsive in between the subsystems. In combination with the popular use of monomer basis sets and the initial guesses for FDE calculations, which usually are isolated-system calculations, this introduces implicit constraints and can be used to obtain quasi-diabatic states (and couplings between them)

of the system. By solving the resulting small, effective eigenvalue problem, one gets access to solutions corresponding to linear combinations of the diabatic states. In the context of electron-transfer (ET) phenomena, this approach is known as FDE-ET. This strategy is conceptually related to methods like Multistate DFT [295] and constrained DFT-CI (CDFT-CI) [296].

FDE-ET was originally formulated for charge-migration processes such as hole transfer reactions, for which a detailed benchmark was presented in Ref. 297. Later studies addressed the role of substituents and central metal on hole transfer in porphyrin dyads [298]. The impact of environmental effects on hole transfer couplings in DNA oligomers was studied in Ref. 299, demonstrating the power of this approach for biological systems. An application along similar lines for ET in the cryptochrome protein from the green alga *Chlamydomonas reinhardtii* was presented in Ref. 300. The couplings, however, were calculated by means of the fragment-orbital density-functional theory scheme in the variant recommended in Ref. 301.

An extension of FDE-ET for charge-separation processes was presented in 2014 [262]. This strategy gives access to accurate long-range charge-transfer (CT) excitation energies, as they are effectively computed as a difference in the energies of two electronic states. It could also be shown that the long-range behavior has the correct  $(-1/R)$  distance behavior and reaches the correct limit. Moreover, it has been demonstrated there that electronic couplings between locally excited (LE) and CT states are accessible when starting from a  $\Delta$ SCF-DFT solution for one of the subsystems involved (rather than from the neutral ground state). It hence offers a valuable alternative to subsystem TDDFT (see Section 6.2.2) for processes involving inter-subsystem charge-transfer phenomena.

The initial FDE-ET developments concentrated on the energetics of charge-transfer processes. But in 2018, the framework was extended in such a way that also the electronic states/densities resulting from the solutions of the model Hamiltonian could be computed

and analyzed [302]. This opened up the route to other classes of problems in which a superposition of several diabatic states can circumvent problems of approximate KS-DFT. In particular, this so-called FDE-diab approach can be applied to calculate accurate spin densities for extended systems or molecular aggregates with radical centers. It avoids both the overdelocalization issues present in KS-DFT (due to the implicit constraints in the underlying FDE calculations) and the effective *overlocalization* present in FDE calculations alone (again due to the constraints) by employing linear combinations of diabatic states. It was shown in Ref. 302 that accurate results can be obtained in radicals formed from dimers with completely localized and completely delocalized spin densities, as well as intermediate situations. Initially, only two diabatic states could be superimposed within FDE-diab calculations, but an extension to multiple states was developed subsequently [303]. Applications of FDE-diab addressed the spin-density asymmetry in the radical cation of the special pair in photosynthetic reaction-center models [304], as well as the spin-density delocalization between a (bacterio-)chlorophyll and a coordinating Histidine [305].

In contrast to FDE-ET/FDE-diab, which use the implicit constraints in approximate FDE calculations to construct the quasi-diabatic states, also explicit constraints have been combined in terms of a Lagrangian formalism in the work on “constrained subsystem density functional theory” (CSDFT) by Pavanello and co-workers [306]. The coupling of different quasi-diabatic states in CSDFT is realized in a similar way as in FDE-ET.

## 6.4 Response Properties

Concerning the computation of properties from the linear-response time-dependent DFT generalization of subsystem DFT, a first application to the calculation of frequency-dependent polarizabilities in 2006 had indicated that the neglect of environmental response is much more critical for this property than for excitation energies [158]. This

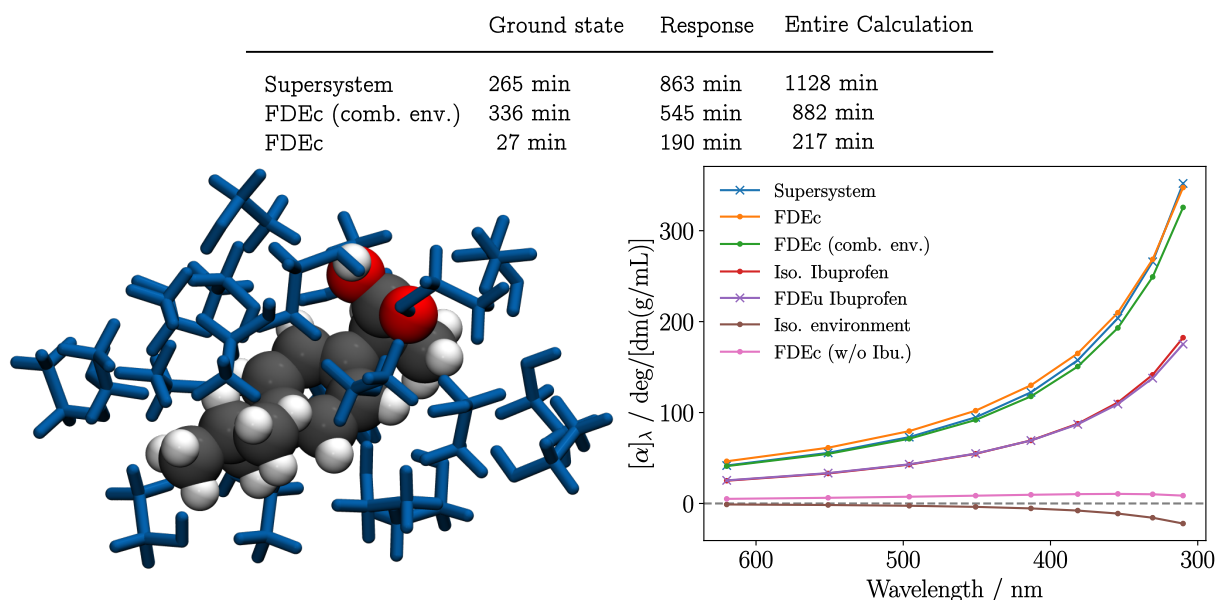


Figure 6: Specific rotations for ibuprofen solvated by 20 ethanol molecules as functions of the wavelength obtained from supersystem KS-DFT calculations (CAM-B3LYP/def2-TZVP) in comparison to subsystem TDDFT (coupled FDE-TDDFT, “FDEc”; CAM-B3LYP/PW91/PW91k/def2-TZVP), either considering the environment as one combined system [FDEc (comb. env.)] or as separate subsystems [FDEc]. In addition, the results for isolated ibuprofen/environment systems, uncoupled FDE-TDDFT calculations on ibuprofen embedded in the ethanol environment, and the FDEc calculations on the environment only are shown to separate the effects of the active molecule and the environment. The geometry was optimized with GFN2-xTB 6.4.1 [?]. Gauge origin invariance was ensured by employing the LG(OI) scheme [309]. The calculations were performed with SERENITY [11] on a dual AMD EPYC 7552 48-core processor with 500 GB of main memory.

finding was corroborated and extended to optical rotatory dispersion (ORD) in 2009 by explicitly considering the coupled response of all subsystems [307]. Crawford *et al.* investigated the ORD and electronic circular dichroism (ECD) spectra of (*p*)-dimethylallene microsolvated by a few water molecules by means of a linear-response variant of CC2-in-DFT embedding [308]. For some of the cases investigated, the results were qualitatively in disagreement with the reference LR-CC2 supersystem calculations.

In later work conducted in one of our groups [218], it could be shown that this is not due to a deficiency in the approximate embedding potential, but to the neglect of the coupled

response between the organic molecule and the solvent; if the environmental response is properly taken into account, the qualitatively correct behaviour is recovered even with approximate NAKPs and monomer basis sets. The study by Niemeyer *et al.* [218] also introduced a damped-response implementation of subsystem TDDFT suited for the computation of electronic absorption and ECD spectra, which can also be employed within the context of projection-based subsystem TDDFT. An illustration of the efficiency of this implementation is provided for a snapshot of methyloxirane solvated by 15 benzene molecules in Ref. 12, for which a fully response-coupled subsystem calculation considering each molecule as a separate fragment only takes about 8 % of the computational time needed in a supermolecular calculation. Jensen and co-workers developed a linear-response generalization [310] of their polarizable FDE method [221], which made use of atomic polarizabilities based on Hirshfeld partitioning and is suited to reproduce coupled polarizabilities.

## 6.5 Magnetic Properties: NMR and EPR

First extensions of sDFT/FDE to the calculation of magnetic properties have already been reviewed in our original article [5]. For treating magnetic properties, it becomes necessary to partition not only the electron density, but also the current density [311]. While originally established for the calculation of nuclear-magnetic resonance (NMR) shielding tensors, the theoretical framework has also been extended to the calculation of NMR spin–spin coupling constant [312]. Olejniczak *et al.* formulated the theory of sDFT/FDE for magnetic properties within a four-component relativistic framework. This allows for the calculation of NMR shielding tensors as well as spin–spin coupling constant of hydrogen-bonded complexes containing heavy atoms. In addition, it makes it possible to systematically analyze the importance of the current-density-dependent contributions. Subsequently, relativistic sDFT/FDE was applied to study the solvent effects on  $\text{MoO}_4^{2-}$

in aqueous solution [162], which includes an analysis of the importance of electronic embedding as well as different relativistic Hamiltonians. An extensive comparative study of solvent effects on the NMR shieldings of heavy-element species in solution is provided in Ref. 143.

EPR hyperfine coupling constants have been investigated by means of subsystem DFT for a model of a guanine hydrochloride monohydrate crystal in Ref. 313. The largest models considered comprised more than 700 QM atoms, and were embedded in a large MM cluster, leading to atomistic QM/MM models with more than 15,000 atoms in total. It could be demonstrated that for this kind of system the large QM cluster size is essential to capture the environment effects on the hyperfine coupling constants. This strategy can even be pushed further in terms of relax-copy cycles for quasi-periodic molecular crystal models [35], as discussed in Section 5.4. In this way, spin densities (though no corresponding hyperfine coupling constants) have been calculated for a thiadiazolo-fused benzotriazinyl radical cluster model with more than 50,000 QM atoms in Ref. 12. While KS-DFT with standard approximations often shows the problem of spin-density overdelocalization for such systems, the corresponding subsystem DFT calculations may suffer from the opposite problem of a too strong spin-density localization. This can be alleviated in terms of the FDE-diab approach by forming linear combinations of several spin-localized configurations, as has been demonstrated for the calculation of hyperfine coupling constants in Ref. 277.

## 6.6 Progress in Wavefunction-in-DFT Embedding

Progress in WF-in-DFT (or WF/DFT) embedding has been made in different directions. Main points concerning the applicability and achievable accuracy are (i) the choice of the wavefunction method, (ii) the choice of the densities for the different parts of the energy expression, or, related to that, the question of self-consistency between the WF and the

DFT part of the calculation, and (iii) extensions to properties beyond the ground-state energy. Several aspects concerning WF-in-DFT have already been discussed in other parts of this review. We will refer to the corresponding sections in the following where appropriate. In particular, we would like to point out that several details have already been mentioned in Section 4.3 in connection with DFET/PFET as developed by Carter and coworkers.

In addition to the three main issues listed above, progress has also been made in the formal analysis of WF-in-DFT embedding methods, which can be approached from different perspectives [40]. Perhaps the most fundamental DFT-type approach to WF-in-DFT embedding was presented by Wesolowski in 2008, regarding the embedded wavefunction as an alternative way of representing the electron density of the active system in terms of a multi-determinantal wavefunction of an interacting system of electrons, rather than a non-interacting, Kohn–Sham-like system [314]. An extension of this work to non-variational embedded wavefunctions followed in 2019 [315]. It was shown that the FDET energy functional can be expanded such that an energy correction from a non-variational, correlated wavefunction method can be employed if it is applied on top of a variational reference method. In addition, two terms linear in the correlation-induced density change  $\Delta\rho(\mathbf{r})$  of the active system appear. The effect of the correlation potential in the context of this formalism was analyzed by Wesolowski as well [316]. Essentially, neglecting the correlation energy functional and potential in the auxiliary system used to represent the active part leads to an energy expression correct to quadratic order in the correlation-induced energy change. A numerical study on interaction energies obtained in this way from DFT-embedded MP2 calculations indicated that hydrogen-bonded and dipole–dipole interaction-dominated complexes are rather well described, while the approximations used failed for interacting (dispersion-type) complexes,  $\pi$ -stacked systems, and in particular for charge-transfer complexes (mainly because of the basis-set incompleteness) [317].

### 6.6.1 Ground States and Ground-State Properties

There has been a tremendous effort to increase the range of wavefunction methods that can be combined with FDE or related methods. A freeze-and-thaw strategy leading to self-consistent DMRG-in-DFT embedding results has been presented in Refs. 318, 319. The effects of mutual density relaxation have been illustrated in that work in terms of the dipole moment of an HCN tetramer, for which the results of a DMRG(40,36)-SCF calculation could be well approximated by an DMRG(20,18)-SCF calculation on an embedded dimer. Several studies involving WF-in-DFT embedding carried out by the Carter group have been discussed above already, see Section 5.4. Moreover, we refer to Section 6.1.2 concerning applications of WF-in-DFT embedding making use of projection techniques.

### 6.6.2 Excited States

Several WF-in-DFT embedding studies addressed the accuracy of excitation energies of chromophores in an environment. In one of the contributions involving our (JN's) lab, we have investigated the effect of the choice of the wavefunction method, ranging from CC2 and CCSD via CCSDR(3) and CASPT2 up to QMC [261]. But also of the type of active-system electron density used to construct the embedding potential for relaxing the environment's density has been analyzed in that study. Besides a state-universal approximation, also state-specific approximations (leading to state-specific embedding potentials) were tested. For the excited states, these were approximately constructed in terms of  $\Delta$ SCF-DFT type solutions (see Section 6.2.1), or directly from the wavefunction-type calculation.

As has already been touched upon in Section 6.2.1, this discussion is complicated by the fact that a state-dependence of the embedding potential for a given system  $A$  in envi-

ronment  $B$  arises both from a change in that environment's density  $\rho_{II}$ , but also from a state-dependent change in the density  $\rho_I$  itself through the non-additive exchange-correlation and non-additive kinetic-energy potentials. This state-dependence of the embedding potential, in turn, leads to a non-orthogonality of the embedded wavefunctions for the states under consideration. It clearly has to be stated that non-orthogonality of the active-system wavefunctions for different electronic states in WF/DFT-embedding is not unphysical, as mentioned in various places [265, 320] and discussed in detail in Ref. 40. The latter work also highlights the conceptual differences to the case of CASSCF calculations, which may be performed in state-specific or state-averaged fashion. More importantly, it also provides some numerical data that quantify non-orthogonality effects. For transition dipole moments, only mild changes due to non-orthogonality are observed. Also the work by Zech *et al.* [320] reported small overlaps between wavefunctions for different electronic states in embedded CASSCF calculations, in line with Ref. 318.

In this context, it is also worth pointing out again that considering the embedding potential as a first-order perturbation, and evaluating its effect on excitation energies in terms of expectation values of the embedding potential amounts to an approximation [260, 321]. Especially concerning the non-additive contributions, however, this approximation benefits from a number of error cancellation effects [260]. One aspect of this, which is relevant also for ground-state calculations, is that inhomogeneity effects on the non-additive energy components are generally small [321]. Hence, the linearization approximation could be established as a well-suited and cost-effective alternative to fully self-consistent WF/DFT calculations [320], which is assumed to work well unless density changes between electronic states become too large. A more extensive comparison of state-universal *vs.* state-specific embedding potentials and various ways to generate the environment densities on which these potentials are based was presented very recently by Fu and Wesolowski [322], showing that both average absolute errors and their standard deviations are reduced when switching from a ground-state polarized environmental density in state-universal em-

bedding potentials to state-specifically polarized densities, but obviously at significantly higher computational cost.

The WF-in-DFT- and WF-in-WF-embedding methods by Höfener and Visscher as discussed in our original review have in the meantime technically been refined and further developed. An implementation of CC-in-DFT for electronic excitations was presented in 2013 and applied for the calculation of solvatochromic shifts [323]. In 2014, Höfener introduced a resolution-of-the-identity-(RI-)CC2 implementation in combination with FDE, which considerably enhanced the efficiency and thus the range of applicability of the method [324]. It was applied to the calculation of local (uncoupled) excitation energies in a CC-in-CC framework. An extension to coupled excitations followed in 2015, where the coupling between CC2-type local excitations was treated within a coupled-cluster-singles-like approximation [325]. Furthermore, a combination of FDE with the conductor-like screening model (COSMO) was presented in this context [326]. For the discussion of subsequent work on analytical gradients by Höfener and co-workers, see Section 6.2.2.

Both ground and local (uncoupled) excited states have been addressed in recent work by Höfener and co-workers employing methods such as Full CI and truncated CI schemes embedded in a DFT environment (or with an additional layer described by MP2) [327], or complete-active-space self-consistent field (CASSCF-)in-DFT embedding [328].

An alternative class of easy-to-use, black-box wavefunction methods for excited states can be defined in terms of the algebraic diagrammatic construction (ADC) scheme for the polarization propagator [329]. A first-time combination of FDET with ADC of second order [ADC(2)] in 2016 showed that complexation-induced shifts in dispersion- or hydrogen-bonded systems could be reproduced with good accuracy [330]. For these calculations, a linearized embedding framework was assumed, so that interaction-energy differences between electronic states could be estimated based on integrals over the corresponding embedding potentials (assumed to be state-universal). Since apparently no

monomer-expansion calculations (i.e., calculations employing only the basis functions of the respective subsystems) could be carried out, and since calculations using supersystem basis sets do not lead to computational advantages, an approximation denoted as “reassembling of the density matrix” (RADM) was introduced. Within that approach, the calculation of the density matrix for the FDE-ADC(2) calculations is only carried out using the basis functions of the active system. An extension to third order [FDE-ADC(3)] followed one year later, and confirmed the rather high accuracy that can be obtained for local excitation energies [331]. Furthermore, this work introduced technical details of the RADM approach. Wesolowski and co-workers also conducted a more extensive test considering 351 excitation energies of 52 different embedded molecules, which confirmed the generally high accuracy for local excitations [332]. In addition, a density-overlap-based criterion was introduced in that work, which could be correlated to errors for certain types of excitations, for which it, in turn, may serve as a diagnostic for the suitability of this methodology. Using the same test set, Hégyel *et al.* [333] performed a comparison of various flavors of ADC(2)-in-PBE embedding and a local domain-based ADC(2) approach. While the latter clearly showed the smallest errors, also frozen-density embedding using approximate NAKPs and PbE resulted in small average absolute errors, considerably smaller than supersystem TDDFT errors.

Besides calculations of excitation energies (and oscillator strengths), also a generalization for the calculation of two-photon absorption cross sections from embedded ADC(2) calculations has been presented [334]. Further efficiency enhancements have been achieved by Treß *et al.*, who combined the uncoupled FDE approach with pair natural orbital (PNO) implementations of the second-order methods CIS(D), ADC(2), and CC2 [19]. An efficient and versatile implementation of embedded wavefunction methods like CIS(D), ADC(2), and CC(2), as well as GW/BSE embedded in DFT together with some proof-of-principle calculations of excitation energies and oscillator strengths was presented in the framework of the SERENITY code in Ref. 12. We also note that a subsystem-based derivation

of GW/BSE and a corresponding implementation (featuring uncoupled excitations) has been developed in Refs. [335, 336].

Excited states of molecules on surfaces or surface models have been studied by Carter and co-workers. In the framework of their DFET, excitation energies and potential-energy surfaces for excited states from embedded wavefunction calculations have been obtained to study the dissociation of H<sub>2</sub> on Au nanoparticles induced by hot electrons [337]. The capped DFET variant has been employed recently to study metal-to-ligand charge-transfer states of a model for a Ru-bipyridine dye covalently bonded to a TiO<sub>2</sub> cluster as a model for a typical dye-sensitized solar cell component [338].

## 7 Conclusions and Outlook

During the past 10 years since the publication of our original review article [5], the field of quantum-chemical embedding methods in general and of sDFT/FDE in particular has seen a tremendous evolution and diversification, up to the point that there is almost a continuous range of methods from QM/continuum and QM/MM methods up to QM/QM methods. Some of these methods may be regarded as simplified versions of sDFT/FDE, in which certain contributions of the interaction terms are either approximated (e.g., electrostatics in terms of distributed multipoles and polarizabilities) or entirely neglected (e.g., non-classical terms).

Important progress in the field of sDFT/FDE has been made in different directions. First, the limitations of previous approximations of the non-additive kinetic-energy terms have been addressed, for instance, by developing new NAKE approximations. Here, it can be expected that recent developments related to non-local KEDFs will have significant impact in sDFT/FDE and will spur the development of new non-local NAKE approximations. Second, strategies for potential reconstruction have been refined and their use is becoming

more and more common. Other strategies, which particularly aim at describing covalently bounded systems, include the 3-FDE or general buffer-fragment methods as well as energy- or density-based many-body expansions combined with sDFT. An alternative that opens up an entirely new avenue is the replacement of the NAKP term by a projection operator in the Kohn-Sham-like equations for sDFT. While this projection-based embedding does, in the context of sDFT (i.e., a DFT-in-DFT embedding) not offer any efficiency advantages compared to a standard Kohn-Sham calculation, it plays important roles as a reference embedding method and in the framework of WF-in-DFT embedding. In this context, however, it has to be kept in mind that PbE is not a strict formal reference for FDE, since it works with projected orbital sets which are, in general, not the orbital sets that minimize the KS-kinetic energies of the subsystems for a given subsystem density.

WF-in-DFT embedding methods based on/related to FDE have benefitted considerably from the PbE strategy, which is, strictly speaking, an orbital- rather than a density-based partitioning. In particular, PbE allows to employ fragmentations cutting through covalent bonds, so that, for instance, active centers and innocent ligands in large transition-metal complexes can be separated. This has motivated strategies for automatizing the selection of the active-orbital set along a reaction path in order to calculate reaction and activation energies. Apart from that, the type of QM methods employed in WF-in-DFT embedding now comprise almost all available correlated electronic-structure methods, including highly correlated ones such as CASPT2, CCSD(T), QMC, DMRG, ASCI, and FCI-QMC. It has also been recognized that it is often not sufficient to improve the description of an active region by moving from DFT-in-DFT embedding to WF-in-DFT embedding. Rather, also the interaction between the WF and the DFT region needs to be improved in general — unless the active system is so large that no significant changes in this interaction occur for the process under study.

In general, numerous implementations of sDFT/FDE and of related density-based embed-

ding methods are nowadays available in numerous quantum-chemical program packages. This facilitates their use in simulations of complex chemical system, which are becoming more and more common. Many new properties are now available from sDFT/FDE and related methods, including the WF-in-DFT embedding methods. As examples, we mention versatile response codes that allow calculations of various types of optical properties and spectra, but also energy gradients for ground and excited states, which make structures optimized with these hybrid methods more easily accessible. In this context, we also note that the usage of approximate FDE as a diabaticization tool made it possible to study phenomena related to charge- and spin-localization, which are often plagued in Kohn–Sham DFT calculations by the overdelocalization problem.

This rapid development has triggered a large number of applications, which, besides “classical” embedding/subsystem setups like dimers, aggregates/clusters, and solvated molecules, comprise more and more complex situations as found in biomolecules, condensed phases/interfaces, and including also impurities as well as adsorbed molecules. We expect that over the coming years, such applications will become more widespread and that the range of complex chemical systems tackled with sDFT/FDE will become even more divers.

## Acknowledgment

We would like to thank Kevin Focke, Lukas Lampe, and Niklas Niemeyer for generating illustrative data for and preparing Figures 3, 6, and 5.

## Conflicts of Interest

There are no conflicts of interest to declare.

## Data Availability Statement

The data of the illustrative calculations provided in this review are available from the corresponding authors upon reasonable request.

## Funding Information

J.N. acknowledges funding from the German Research Foundation (DFG) through CRC 1459 (Project A03 – 433682494). C.R.J. acknowledges funding from the German Research Foundation (DFG) through projects Suresoft (JA 2329/7-1) and CompRIXS (JA 2329/6-1).

## References

- [1] C. Kaspar, B. J. Ravoo, W. G. van der Wiel, S. V. Wegner, and W. H. P. Pernice, *The rise of intelligent matter*, Nature **594**, 345 (2021).
- [2] R. Schade et al., *Towards electronic structure-based ab-initio molecular dynamics simulations with hundreds of millions of atoms*, Parallel Comput. **111**, 102920 (2022).
- [3] M. S. Gordon, editor, *Fragmentation: Toward Accurate Calculations on Complex Molecular Systems*, Wiley, Hoboken, NJ, 1st edition, 2017.
- [4] A. Wasserman and M. Pavanello, *Quantum embedding electronic structure methods*, Int. J. Quantum Chem. **120**, e26495 (2020).
- [5] Ch. R. Jacob and J. Neugebauer, *Subsystem density-functional theory*, WIREs Comput. Mol. Sci. **4**, 325 (2014).

- [6] T. A. Wesolowski and A. Warshel, *Frozen Density Functional Approach for ab Initio Calculations of Solvated Molecules*, J. Phys. Chem. **97**, 8050 (1993).
- [7] T. A. Wesolowski, S. Shedge, and X. Zhou, *Frozen-Density Embedding Strategy for Multilevel Simulations of Electronic Structure*, Chem. Rev. **115**, 5891 (2015).
- [8] N. Ricardi, C. E. González-Espinoza, and T. A. Wesolowski, *N-representability of the target density in Frozen-Density Embedding Theory based methods: Numerical significance and its relation to electronic polarization*, J. Chem. Phys. **157**, 064108 (2022).
- [9] T. A. Wesolowski, *Is the non-additive kinetic potential always equal to the difference of effective potentials from inverting the Kohn–Sham equation?*, J. Chem. Phys. **157**, 081102 (2022).
- [10] M. Jansen, N. N. T. Minh, E. D. Hedegård, and C. König, Quantum-derived embedding schemes for local excitations, in *Chemical Modelling*, pages 24–60, Royal Society of Chemistry, 2022, DOI: 10.1039/9781839169342-00024.
- [11] J. P. Unsleber, T. Dresselhaus, K. Klahr, D. Schnieders, M. Böckers, D. Barton, and J. Neugebauer, *Serenity: A subsystem quantum chemistry program*, J. Comput. Chem. **39**, 788 (2018).
- [12] N. Niemeyer et al., *The subsystem quantum chemistry program Serenity*, WIREs Comput. Mol. Sci. , e1647 (2023), in press, DOI: 10.1002/wcms.1647.
- [13] A. Genova, D. Ceresoli, A. Krishtal, O. Andreussi, R. A. DiStasio, and M. Pavanello, *eQE: An open-source density functional embedding theory code for the condensed phase*, Int. J. Quantum Chem. **117**, e25401 (2017).
- [14] W. Mi, X. Shao, A. Genova, D. Ceresoli, and M. Pavanello, *eQE 2.0: Subsystem DFT beyond GGA functionals*, Comput. Phys. Commun. **269**, 108122 (2021).

- [15] S. Andermatt, J. Cha, F. Schiffmann, and J. VandeVondele, *Combining Linear-Scaling DFT with Subsystem DFT in Born–Oppenheimer and Ehrenfest Molecular Dynamics Simulations: From Molecules to a Virus in Solution*, *J. Chem. Theory Comput.* **12**, 3214 (2016).
- [16] V. V. Rybkin, *Formulation and Implementation of Density Functional Embedding Theory Using Products of Basis Functions*, *J. Chem. Theory Comput.* **17**, 3995 (2021).
- [17] S. Höfener, *The KOALA program: Wavefunction frozen-density embedding*, *Int. J. Quantum Chem.* **121**, e26351 (2021).
- [18] M. Sharma and M. Sierka, *Efficient Implementation of Density Functional Theory Based Embedding for Molecular and Periodic Systems Using Gaussian Basis Functions*, *J. Chem. Theory Comput.* **18**, 6892 (2022).
- [19] R. S. Treß, J. Liu, C. Hättig, and S. Höfener, *Pushing the limits: Efficient wavefunction methods for excited states in complex systems using frozen-density embedding*, *J. Chem. Phys.* **157**, 204101 (2022).
- [20] H.-J. Werner et al., *The Molpro quantum chemistry package*, *J. Chem. Phys.* **152**, 144107 (2020).
- [21] E. Epifanovsky et al., *Software for the frontiers of quantum chemistry: An overview of developments in the Q-Chem 5 package*, *J. Chem. Phys.* **155**, 084801 (2021).
- [22] A. Goez and J. Neugebauer, *Embedding Methods in Quantum Chemistry*, in *Frontiers of Quantum Chemistry*, edited by M. J. Wójcik, H. Nakatsuji, B. Kirtman, and Y. Ozaki, pages 139–179, Springer, Singapore, 2018, DOI: 10.1007/978-981-10-5651-2\_7.
- [23] Q. Sun and G. K.-L. Chan, *Quantum Embedding Theories*, *Acc. Chem. Res.* **49**, 2705 (2016).

- [24] L. O. Jones, M. A. Mosquera, G. C. Schatz, and M. A. Ratner, *Embedding Methods for Quantum Chemistry: Applications from Materials to Life Sciences*, J. Am. Chem. Soc. **142**, 3281 (2020).
- [25] A. Krishtal, D. Sinha, A. Genova, and M. Pavanello, *Subsystem density-functional theory as an effective tool for modeling ground and excited states, their dynamics and many-body interactions*, J. Phys.: Condens. Matter **27**, 183202 (2015).
- [26] P. Elliott, K. Burke, M. H. Cohen, and A. Wasserman, *Partition density-functional theory*, Phys. Rev. A **82**, 024501 (2010).
- [27] J. Nafziger, Q. Wu, and A. Wasserman, *Molecular binding energies from partition density functional theory*, J. Chem. Phys. **135**, 234101 (2011).
- [28] R. Tang, J. Nafziger, and A. Wasserman, *Fragment occupations in partition density functional theory*, Phys. Chem. Chem. Phys. **14**, 7780 (2012).
- [29] M. A. Mosquera, D. Jensen, and A. Wasserman, *Fragment-Based Time-Dependent Density Functional Theory*, Phys. Rev. Lett. **111**, 023001 (2013).
- [30] M. A. Mosquera and A. Wasserman, *Partition density functional theory and its extension to the spin-polarized case*, Mol. Phys. **111**, 505 (2013).
- [31] J. Nafziger and A. Wasserman, *Density-Based Partitioning Methods for Ground-State Molecular Calculations*, J. Phys. Chem. A **118**, 7623 (2014).
- [32] J. Nafziger and A. Wasserman, *Fragment-based treatment of delocalization and static correlation errors in density-functional theory*, J. Chem. Phys. **143**, 234105 (2015).
- [33] S. Gómez, J. Nafziger, A. Restrepo, and A. Wasserman, *Partition-DFT on the water dimer*, J. Chem. Phys. **146**, 074106 (2017).
- [34] K. Zhang and A. Wasserman, *Split electrons in partition density functional theory*, J. Chem. Phys. **156**, 224113 (2022).

- [35] P. Eschenbach and J. Neugebauer, *Subsystem density-functional theory: A reliable tool for spin-density based properties*, J. Chem. Phys. **157**, 130902 (2022).
- [36] S. J. R. Lee, M. Welborn, F. R. Manby, and T. F. Miller, *Projection-Based Wavefunction-in-DFT Embedding*, Acc. Chem. Res. **52**, 1359 (2019).
- [37] M. Bensberg and J. Neugebauer, *Density functional theory based embedding approaches for transition-metal complexes*, Phys. Chem. Chem. Phys. **22**, 26093 (2020).
- [38] F. Libisch, C. Huang, and E. A. Carter, *Embedded Correlated Wavefunction Schemes: Theory and Applications*, Acc. Chem. Res. **47**, 2768 (2014).
- [39] K. Yu, C. M. Krauter, J. M. Dieterich, and E. A. Carter, *Density and Potential Functional Embedding: Theory and Practice*, in *Fragmentation*, edited by M. S. Gordon, pages 81–117, John Wiley & Sons, Ltd, 2017.
- [40] T. Dresselhaus and J. Neugebauer, *Part and whole in wavefunction/DFT embedding*, Theor. Chem. Acc. **134**, 1 (2015).
- [41] M. De Santis, D. Sorbelli, V. Vallet, A. S. P. Gomes, L. Storchi, and L. Bellaspasi, *Frozen-Density Embedding for Including Environmental Effects in the Dirac-Kohn–Sham Theory: An Implementation Based on Density Fitting and Prototyping Techniques*, J. Chem. Theory Comput. **18**, 5992 (2022).
- [42] V. V. Karasiev and S. B. Trickey, Chapter Nine - Frank Discussion of the Status of Ground-State Orbital-Free DFT, in *Advances in Quantum Chemistry*, edited by J. R. Sabin and R. Cabrera-Trujillo, volume 71 of *Concepts of Mathematical Physics in Chemistry: A Tribute to Frank E. Harris - Part A*, pages 221–245, Academic Press, 2015, DOI: 10.1016/bs.aiq.2015.02.004.
- [43] J. M. Dieterich, W. C. Witt, and E. A. Carter, *libKEDF: An accelerated library of kinetic energy density functionals*, J. Comput. Chem. **38**, 1552 (2017).

- [44] L. A. Constantin, E. Fabiano, and F. Della Sala, *Modified Fourth-Order Kinetic Energy Gradient Expansion with Hartree Potential-Dependent Coefficients*, J. Chem. Theory Comput. **13**, 4228 (2017).
- [45] W. C. Witt, B. G. d. Rio, J. M. Dieterich, and E. A. Carter, *Orbital-free density functional theory for materials research*, J. Mater. Res. **33**, 777 (2018).
- [46] K. Luo, V. V. Karasiev, and S. B. Trickey, *A simple generalized gradient approximation for the noninteracting kinetic energy density functional*, Phys. Rev. B **98**, 041111 (2018).
- [47] J. Seino, R. Kageyama, M. Fujinami, Y. Iwabata, and H. Nakai, *Semi-local machine-learned kinetic energy density functional with third-order gradients of electron density*, J. Chem. Phys. **148**, 241705 (2018).
- [48] W. Mi, A. Genova, and M. Pavanello, *Nonlocal kinetic energy functionals by functional integration*, J. Chem. Phys. **148**, 184107 (2018).
- [49] W. Mi and M. Pavanello, *Orbital-free density functional theory correctly models quantum dots when asymptotics, nonlocality, and nonhomogeneity are accounted for*, Phys. Rev. B **100**, 041105 (2019).
- [50] W. C. Witt and E. A. Carter, *Kinetic energy density of nearly free electrons. I. Response functionals of the external potential*, Phys. Rev. B **100**, 125106 (2019).
- [51] S. A. Ghasemi and T. D. Kühne, *Artificial neural networks for the kinetic energy functional of non-interacting fermions*, J. Chem. Phys. **154**, 074107 (2021).
- [52] S. Kumar, E. L. Borda, B. Sadigh, S. Zhu, S. Hamel, B. Gallagher, V. Bulatov, J. Klepeis, and A. Samanta, *Accurate parameterization of the kinetic energy functional*, J. Chem. Phys. **156**, 024110 (2022).

- [53] K. Ryczko, S. J. Wetzel, R. G. Melko, and I. Tamblyn, *Toward Orbital-Free Density Functional Theory with Small Data Sets and Deep Learning*, J. Chem. Theory Comput. **18**, 1122 (2022).
- [54] E. Fabiano, F. Sarcinella, L. A. Constantin, and F. Della Sala, *Kinetic Energy Density Functionals Based on a Generalized Screened Coulomb Potential: Linear Response and Future Perspectives*, Computation **10**, 30 (2022).
- [55] A. Lembarki and H. Chermette, *Obtaining a gradient-corrected kinetic-energy functional from the Perdew-Wang exchange functional*, Phys. Rev. A **50**, 5328 (1994).
- [56] S. Laricchia, E. Fabiano, L. A. Constantin, and F. Della Sala, *Generalized Gradient Approximations of the Noninteracting Kinetic Energy from the Semiclassical Atom Theory: Rationalization of the Accuracy of the Frozen Density Embedding Theory for Nonbonded Interactions*, J. Chem. Theory Comput. **7**, 2439 (2011).
- [57] A. Genova, D. Ceresoli, and M. Pavanello, *Periodic subsystem density-functional theory*, J. Chem. Phys. **141**, 174101 (2014).
- [58] S. A. Grimmel, T. Q. Teodoro, and L. Visscher, *Is it worthwhile to go beyond the local-density approximation in subsystem density functional theory?*, Int. J. Quantum Chem. **120**, e26111 (2020).
- [59] S. Laricchia, L. A. Constantin, E. Fabiano, and F. Della Sala, *Laplacian-Level Kinetic Energy Approximations Based on the Fourth-Order Gradient Expansion: Global Assessment and Application to the Subsystem Formulation of Density Functional Theory*, J. Chem. Theory Comput. **10**, 164 (2014).
- [60] L.-W. Wang and M. P. Teter, *Kinetic-energy functional of the electron density*, Phys. Rev. B **45**, 13196 (1992).
- [61] W. Mi and M. Pavanello, *Nonlocal Subsystem Density Functional Theory*, J. Phys. Chem. Lett. **11**, 272 (2020).

- [62] F. Sarcinella, E. Fabiano, L. A. Constantin, and F. Della Sala, *Nonlocal kinetic energy functionals in real space using a Yukawa-potential kernel: Properties, linear response, and model functionals*, Phys. Rev. B **103**, 155127 (2021).
- [63] F. Sarcinella, S. Śmiga, F. D. Sala, and E. Fabiano, *Gaussian expansion of Yukawa non-local kinetic energy functionals: Application to metal clusters*, Int. J. Quantum Chem. **n/a**, e27188 (2023).
- [64] Ch. R. Jacob, S. M. Beyhan, and L. Visscher, *Exact functional derivative of the nonadditive kinetic-energy bifunctional in the long-distance limit*, J. Chem. Phys. **126**, 234116 (2007).
- [65] J. M. Garcia Lastra, J. W. Kaminski, and T. A. Wesolowski, *Orbital-free effective embedding potential at nuclear cusps*, J. Chem. Phys. **129**, 074107 (2008).
- [66] E. Polak, C. E. González-Espinoza, M. J. Gander, and T. A. Wesolowski, *A non-decomposable approximation on the complete density function space for the non-additive kinetic potential*, J. Chem. Phys. **156**, 044103 (2022).
- [67] E. Polak, T. Englert, M. J. Gander, and T. A. Wesolowski, *Symmetrized non-decomposable approximations of the non-additive kinetic energy functional*, J. Chem. Phys. **158**, 174107 (2023).
- [68] X. Shao, W. Mi, and M. Pavanello, *GGA-Level Subsystem DFT Achieves Sub-kcal/mol Accuracy Intermolecular Interactions by Mimicking Nonlocal Functionals*, J. Chem. Theory Comput. **17**, 3455 (2021).
- [69] K. Jiang, J. Nafziger, and A. Wasserman, *Non-additive non-interacting kinetic energy of rare gas dimers*, J. Chem. Phys. **148**, 104113 (2018).
- [70] T. A. Wesolowski, *Density functional theory with approximate kinetic energy functionals applied to hydrogen bonds*, J. Chem. Phys. **106**, 8516 (1997).

- [71] Ch. R. Jacob, T. A. Wesolowski, and L. Visscher, *Orbital-free embedding applied to the calculation of induced dipole moments in  $CO_2 \cdots X$  ( $X = He, Ne, Ar, Kr, Xe, Hg$ ) van der Waals complexes*, J. Chem. Phys. **123**, 174104 (2005).
- [72] S. Laricchia, E. Fabiano, and F. Della Sala, *Frozen density embedding with hybrid functionals*, J. Chem. Phys. **133**, 164111 (2010).
- [73] S. Laricchia, E. Fabiano, and F. Della Sala, *Frozen density embedding calculations with the orbital-dependent localized Hartree–Fock Kohn–Sham potential*, Chem. Phys. Lett. **518**, 114 (2011).
- [74] S. Laricchia, E. Fabiano, and F. D. Sala, *On the accuracy of frozen density embedding calculations with hybrid and orbital-dependent functionals for non-bonded interaction energies*, J. Chem. Phys. **137**, 014102 (2012).
- [75] S. Śmiga, E. Fabiano, S. Laricchia, L. A. Constantin, and F. Della Sala, *Subsystem density functional theory with meta-generalized gradient approximation exchange-correlation functionals*, J. Chem. Phys. **142**, 154121 (2015).
- [76] S. Śmiga, E. Fabiano, L. A. Constantin, and F. Della Sala, *Laplacian-dependent models of the kinetic energy density: Applications in subsystem density functional theory with meta-generalized gradient approximation functionals*, J. Chem. Phys. **146**, 064105 (2017).
- [77] A. Genova, D. Ceresoli, and M. Pavanello, *Avoiding fractional electrons in subsystem DFT based ab-initio molecular dynamics yields accurate models for liquid water and solvated OH radical*, J. Chem. Phys. **144**, 234105 (2016).
- [78] E. Fabiano, S. Laricchia, and F. Della Sala, *Frozen density embedding with non-integer subsystems’ particle numbers*, J. Chem. Phys. **140**, 114101 (2014).
- [79] A. Schulz and Ch. R. Jacob, *Description of intermolecular charge transfer with subsystem density-functional theory*, J. Chem. Phys. **151**, 131103 (2019).

- [80] S. Liu and P. W. Ayers, *Functional derivative of noninteracting kinetic energy density functional*, Phys. Rev. A **70**, 022501 (2004).
- [81] R. Cuevas-Saavedra, P. W. Ayers, and V. N. Staroverov, *Kohn–Sham exchange–correlation potentials from second-order reduced density matrices*, J. Chem. Phys. **143**, 244116 (2015).
- [82] I. G. Ryabinkin, S. V. Kohut, and V. N. Staroverov, *Reduction of Electronic Wave Functions to Kohn–Sham Effective Potentials*, Phys. Rev. Lett. **115**, 083001 (2015).
- [83] R. Cuevas-Saavedra and V. N. Staroverov, *Exact expressions for the Kohn–Sham exchange–correlation potential in terms of wave-function-based quantities*, Mol. Phys. **114**, 1050 (2016).
- [84] K. Finzel, P. W. Ayers, and P. Bultinck, *A simple algorithm for the Kohn–Sham inversion problem applicable to general target densities*, Theor. Chem. Acc. **137**, 30 (2018).
- [85] X. Zhang and E. A. Carter, *Kohn–Sham potentials from electron densities using a matrix representation within finite atomic orbital basis sets*, J. Chem. Phys. **148**, 034105 (2018).
- [86] B. Kanungo, P. M. Zimmerman, and V. Gavini, *Exact exchange–correlation potentials from ground-state electron densities*, Nat. Commun. **10**, 1 (2019).
- [87] T. J. Callow, N. N. Lathiotakis, and N. I. Gidopoulos, *Density-inversion method for the Kohn–Sham potential: Role of the screening density*, J. Chem. Phys. **152**, 164114 (2020).
- [88] A. Kumar and M. K. Harbola, *A general penalty method for density-to-potential inversion*, Int. J. Quantum Chem. **120**, e26400 (2020).

- [89] S. Nam, R. J. McCarty, H. Park, and E. Sim, *KS-pies: Kohn–Sham inversion toolkit*, J. Chem. Phys. **154**, 124122 (2021).
- [90] J. B. Stückrath and F. A. Bischoff, *Reduction of Hartree–Fock Wavefunctions to Kohn–Sham Effective Potentials Using Multiresolution Analysis*, J. Chem. Theory Comput. **17**, 1408 (2021).
- [91] Y. Oueis and V. N. Staroverov, *Reconstruction of Exchange–Correlation Potentials from Their Matrix Representations*, J. Chem. Theory Comput. **18**, 6092 (2022).
- [92] Y. Shi, V. H. Chávez, and A. Wasserman, *n2v: A density-to-potential inversion suite. A sandbox for creating, testing, and benchmarking density functional theory inversion methods*, WIREs Comput. Mol. Sci. **12**, e1617 (2022).
- [93] T. Gould, *Toward routine Kohn–Sham inversion using the “Lieb-response” approach*, J. Chem. Phys. **158**, 064102 (2023).
- [94] Y. Oueis, G. N. Sizov, and V. N. Staroverov, *Local Potentials Reconstructed within Linearly Independent Product Basis Sets of Increasing Size*, J. Phys. Chem. A **127**, 2664 (2023).
- [95] D. S. Jensen and A. Wasserman, *Numerical methods for the inverse problem of density functional theory*, Int. J. Quantum Chem. **118**, e25425 (2018).
- [96] Y. Shi and A. Wasserman, *Inverse Kohn–Sham Density Functional Theory: Progress and Challenges*, J. Phys. Chem. Lett. **12**, 5308 (2021).
- [97] M. Banafsheh and T. A. Wesolowski, *Nonadditive kinetic potentials from inverted Kohn–Sham problem*, Int. J. Quantum Chem. **118**, e25410 (2018).
- [98] D. Schnieders and J. Neugebauer, *Accurate embedding through potential reconstruction: A comparison of different strategies*, J. Chem. Phys. **149**, 054103 (2018).

- [99] S. Fux, Ch. R. Jacob, J. Neugebauer, L. Visscher, and M. Reiher, *Accurate frozen-density embedding potentials as a first step towards a subsystem description of covalent bonds*, J. Chem. Phys. **132**, 164101 (2010).
- [100] P. de Silva and T. A. Wesolowski, *Exact non-additive kinetic potentials in realistic chemical systems*, J. Chem. Phys. **137**, 094110 (2012).
- [101] P. de Silva and T. A. Wesolowski, *Pure-state noninteracting  $v$ -representability of electron densities from Kohn-Sham calculations with finite basis sets*, Phys. Rev. A **85**, 032518 (2012).
- [102] J. Nafziger, K. Jiang, and A. Wasserman, *Accurate Reference Data for the Nonadditive, Noninteracting Kinetic Energy in Covalent Bonds*, J. Chem. Theory Comput. **13**, 577 (2017).
- [103] Y. G. Khait and M. R. Hoffmann, *On the Orthogonality of Orbitals in Subsystem Kohn–Sham Density Functional Theory*, in *Annual Reports in Computational Chemistry*, edited by R. A. Wheeler, volume Volume 8, pages 53–70, Elsevier, 2012.
- [104] P. K. Tamukong, Y. G. Khait, and M. R. Hoffmann, *Density Differences in Embedding Theory with External Orbital Orthogonality*, J. Phys. Chem. A **118**, 9182 (2014).
- [105] D. V. Chulhai and L. Jensen, *Frozen Density Embedding with External Orthogonality in Delocalized Covalent Systems*, J. Chem. Theory Comput. **11**, 3080 (2015).
- [106] J. P. Unsleber, J. Neugebauer, and Ch. R. Jacob, *No need for external orthogonality in subsystem density-functional theory*, Phys. Chem. Chem. Phys. **18**, 21001 (2016).
- [107] D. G. Artiukhin, Ch. R. Jacob, and J. Neugebauer, *Excitation energies from frozen-density embedding with accurate embedding potentials*, J. Chem. Phys. **142**, 234101 (2015).

- [108] C. Huang, M. Pavone, and E. A. Carter, *Quantum mechanical embedding theory based on a unique embedding potential*, J. Chem. Phys. **134**, 154110 (2011).
- [109] C. Huang and E. A. Carter, *Potential-functional embedding theory for molecules and materials*, J. Chem. Phys. **135**, 194104 (2011).
- [110] Q. Wu and W. Yang, *A direct optimization method for calculating density functionals and exchange–correlation potentials from electron densities*, J. Chem. Phys. **118**, 2498 (2003).
- [111] K. Yu, F. Libisch, and E. A. Carter, *Implementation of density functional embedding theory within the projector-augmented-wave method and applications to semiconductor defect states*, J. Chem. Phys. **143**, 102806 (2015).
- [112] J. Cheng, F. Libisch, K. Yu, M. Chen, J. M. Dieterich, and E. A. Carter, *Potential Functional Embedding Theory at the Correlated Wave Function Level. 1. Mixed Basis Set Embedding*, J. Chem. Theory Comput. **13**, 1067 (2017).
- [113] J. Cheng, K. Yu, F. Libisch, J. M. Dieterich, and E. A. Carter, *Potential Functional Embedding Theory at the Correlated Wave Function Level. 2. Error Sources and Performance Tests*, J. Chem. Theory Comput. **13**, 1081 (2017).
- [114] K. Yu and E. A. Carter, *Extending density functional embedding theory for covalently bonded systems*, Proc. Natl. Acad. Sci. U. S. A. **114**, E10861 (2017).
- [115] J. M. P. Martirez and E. A. Carter, *Projector-Free Capped-Fragment Scheme within Density Functional Embedding Theory for Covalent and Ionic Compounds*, J. Chem. Theory Comput. **17**, 4105 (2021).
- [116] Ch. R. Jacob and L. Visscher, *A subsystem density-functional theory approach for the quantum chemical treatment of proteins*, J. Chem. Phys. **128**, 155102 (2008).

- [117] C. E. Hoyer, D. B. Williams-Young, C. Huang, and X. Li, *Embedding non-collinear two-component electronic structure in a collinear quantum environment*, J. Chem. Phys. **150**, 174114 (2019).
- [118] C. Huang, *Extending the density functional embedding theory to finite temperature and an efficient iterative method for solving for embedding potentials*, J. Chem. Phys. **144**, 124106 (2016).
- [119] C. Huang, *Embedded Cluster Density Approximation for Exchange–Correlation Energy: A Natural Extension of the Local Density Approximation*, J. Chem. Theory Comput. **14**, 6211 (2018).
- [120] C. Huang, *Correction to “Embedded Cluster Density Approximation for Exchange–Correlation Energy: A Natural Extension of the Local Density Approximation”*, J. Chem. Theory Comput. **15**, 6550 (2019).
- [121] Y.-C. Chi, M. Shaban Tameh, and C. Huang, *Efficient Embedded Cluster Density Approximation Calculations with an Orbital-Free Treatment of Environments*, J. Chem. Theory Comput. **17**, 2737 (2021).
- [122] C. Huang, *Wavelength-decomposition-based embedded cluster density approximation for systems with nonlocal electron correlation*, Int. J. Quantum Chem. **120**, e26347 (2020).
- [123] C. Huang, A. B. Muñoz-García, and M. Pavone, *Effective scheme for partitioning covalent bonds in density-functional embedding theory: From molecules to extended covalent systems*, J. Chem. Phys. **145**, 244103 (2016).
- [124] C. Huang, *Patching the Exchange-Correlation Potential in Density Functional Theory*, J. Chem. Theory Comput. **12**, 2224 (2016).

- [125] A. Massolle and J. Neugebauer, *Subsystem density-functional theory for interacting open-shell systems: spin densities and magnetic exchange couplings*, Faraday Discuss. **224**, 201 (2020).
- [126] A. Massolle and J. Neugebauer, *Pragmatic Improvement of Magnetic Exchange Couplings from Subsystem Density-Functional Theory through Orthogonalization of Subsystem Orbitals*, J. Phys. Chem. C **125**, 6176 (2021).
- [127] D. Schlüns, K. Klahr, C. Mück-Lichtenfeld, L. Visscher, and J. Neugebauer, *Subsystem-DFT potential-energy curves for weakly interacting systems*, Phys. Chem. Chem. Phys. **17**, 14323 (2015).
- [128] T. A. Wesolowski, H. Chermette, and J. Weber, *Accuracy of approximate kinetic energy functionals in the model of Kohn-Sham equations with constrained electron density: The FH—NCH complex as a test case*, J. Chem. Phys. **105**, 9182 (1996).
- [129] S. Laricchia, E. Fabiano, and F. D. Sala, *Semilocal and hybrid density embedding calculations of ground-state charge-transfer complexes*, J. Chem. Phys. **138**, 124112 (2013).
- [130] Y. Zhao and D. G. Truhlar, *Design of Density Functionals That Are Broadly Accurate for Thermochemistry, Thermochemical Kinetics, and Nonbonded Interactions*, J. Phys. Chem. A **109**, 5656 (2005).
- [131] Y. Zhao and D. G. Truhlar, *Benchmark Databases for Nonbonded Interactions and Their Use To Test Density Functional Theory*, J. Chem. Theory Comput. **1**, 415 (2005).
- [132] E. Fabiano, L. A. Constantin, and F. Della Sala, *Wave Function and Density Functional Theory Studies of Dihydrogen Complexes*, J. Chem. Theory Comput. **10**, 3151 (2014).

- [133] P. Jurečka, J. Šponer, J. Černý, and P. Hobza, *Benchmark database of accurate (MP2 and CCSD(T) complete basis set limit) interaction energies of small model complexes, DNA base pairs, and amino acid pairs*, Phys. Chem. Chem. Phys. **8**, 1985 (2006).
- [134] L. Gráfová, M. Pitoňák, J. Řezáč, and P. Hobza, *Comparative Study of Selected Wave Function and Density Functional Methods for Noncovalent Interaction Energy Calculations Using the Extended S22 Data Set*, J. Chem. Theory Comput. **6**, 2365 (2010).
- [135] J. Řezáč, K. E. Riley, and P. Hobza, *S66: A Well-balanced Database of Benchmark Interaction Energies Relevant to Biomolecular Structures*, J. Chem. Theory Comput. **7**, 2427 (2011).
- [136] J. Řezáč and P. Hobza, *Describing Noncovalent Interactions beyond the Common Approximations: How Accurate Is the “Gold Standard,” CCSD(T) at the Complete Basis Set Limit?*, J. Chem. Theory Comput. **9**, 2151 (2013).
- [137] K. Klahr, D. Schlüns, and J. Neugebauer, *Geometry Optimizations in a Subsystem Density Functional Theory Formalism: A Benchmark Study*, J. Chem. Theory Comput. **14**, 5631 (2018).
- [138] S. Grimme, J. Antony, S. Ehrlich, and H. Krieg, *A consistent and accurate ab initio parametrization of density functional dispersion correction (DFT-D) for the 94 elements H-Pu*, J. Chem. Phys. **132**, 154104 (2010).
- [139] S. Grimme, S. Ehrlich, and L. Goerigk, *Effect of the damping function in dispersion corrected density functional theory*, J. Comput. Chem. **32**, 1456–1465 (2011).
- [140] D. Schlüns, M. Franchini, A. W. Götz, J. Neugebauer, Ch. R. Jacob, and L. Visscher, *Analytical gradients for subsystem density functional theory within the slater-*

- function-based amsterdam density functional program*, J. Comput. Chem. **38**, 238 (2017).
- [141] Ch. R. Jacob, J. Neugebauer, and L. Visscher, *A flexible implementation of frozen-density embedding for use in multilevel simulations*, J. Comput. Chem. **29**, 1011 (2008).
- [142] S. Schürmann, J. R. Vornweg, M. Wolter, and Ch. R. Jacob, *Accurate quantum-chemical fragmentation calculations for ion–water clusters with the density-based many-body expansion*, Phys. Chem. Chem. Phys. **25**, 736 (2023).
- [143] M. Olejniczak, A. Antušek, and M. Jaszuński, *Relativistic frozen density embedding calculations of solvent effects on the nuclear magnetic resonance shielding constants of transition metal nuclei*, Int. J. Quantum Chem. **121**, e26789 (2021).
- [144] A. Genova and M. Pavanello, *Exploiting the locality of periodic subsystem density-functional theory: efficient sampling of the Brillouin zone*, J. Phys.: Condens. Matter **27**, 495501 (2015).
- [145] Q. Zhao, X. Zhang, J. M. P. Martirez, and E. A. Carter, *Benchmarking an Embedded Adaptive Sampling Configuration Interaction Method for Surface Reactions: H<sub>2</sub> Desorption from and CH<sub>4</sub> Dissociation on Cu(111)*, J. Chem. Theory Comput. **16**, 7078 (2020).
- [146] M. Wolter, M. von Looz, H. Meyerhenke, and Ch. R. Jacob, *Systematic Partitioning of Proteins for Quantum-Chemical Fragmentation Methods Using Graph Algorithms*, J. Chem. Theory Comput. **17**, 1355 (2021).
- [147] R. Sabatini, T. Gorni, and S. de Gironcoli, *Nonlocal van der Waals density functional made simple and efficient*, Phys. Rev. B **87**, 041108 (2013).
- [148] F. Furche and T. Van Voorhis, *Fluctuation-dissipation theorem density-functional theory*, J. Chem. Phys. **122**, 164106 (2005).

- [149] R. Kevorkyants, H. Eshuis, and M. Pavanello, *FDE-vdW: A van der Waals inclusive subsystem density-functional theory*, J. Chem. Phys. **141**, 044127 (2014).
- [150] D. Sinha and M. Pavanello, *Exact kinetic energy enables accurate evaluation of weak interactions by the FDE-vdW method*, J. Chem. Phys. **143**, 084120 (2015).
- [151] J. M. Herbert, *Fantasy versus reality in fragment-based quantum chemistry*, J. Chem. Phys. **151**, 170901 (2019).
- [152] D. Schmitt-Monreal and Ch. R. Jacob, *Frozen-density embedding-based many-body expansions*, Int. J. Quantum Chem. **120**, e26228 (2020).
- [153] L. Scholz and J. Neugebauer, *Protein Response Effects on Cofactor Excitation Energies from First Principles: Augmenting Subsystem Time-Dependent Density-Functional Theory with Many-Body Expansion Techniques*, J. Chem. Theory Comput. **17**, 6105 (2021).
- [154] D. Schmitt-Monreal and Ch. R. Jacob, *Density-Based Many-Body Expansion as an Efficient and Accurate Quantum-Chemical Fragmentation Method: Application to Water Clusters*, J. Chem. Theory Comput. **17**, 4144 (2021).
- [155] J. Neugebauer, M. J. Louwerse, E. J. Baerends, and T. A. Wesolowski, *The merits of the frozen-density embedding scheme to model solvatochromic shifts*, J. Chem. Phys. **122**, 094115 (2005).
- [156] J. Neugebauer, Ch. R. Jacob, T. A. Wesolowski, and E. J. Baerends, *An Explicit Quantum Chemical Method for Modeling Large Solvation Shells Applied to Aminocoumarin C151*, J. Phys. Chem. A **109**, 7805 (2005).
- [157] J. Neugebauer, M. J. Louwerse, P. Belanzoni, T. A. Wesolowski, and E. J. Baerends, *Modeling solvent effects on electron-spin-resonance hyperfine couplings by frozen-density embedding*, J. Chem. Phys. **123**, 114101 (2005).

- [158] Ch. R. Jacob, J. Neugebauer, L. Jensen, and L. Visscher, *Comparison of frozen-density embedding and discrete reaction field solvent models for molecular properties*, Phys. Chem. Chem. Phys. **8**, 2349 (2006).
- [159] R. E. Bulo, Ch. R. Jacob, and L. Visscher, *NMR Solvent Shifts of Acetonitrile from Frozen Density Embedding Calculations*, J. Phys. Chem. A **112**, 2640 (2008).
- [160] N. Middendorf, K. Krause, and S. Höfener, *Solvatochromic shifts of Br<sub>2</sub> and I<sub>2</sub> in water cages of type 5<sup>12</sup>, 5<sup>12</sup>6<sup>2</sup>, 5<sup>12</sup>6<sup>3</sup>, and 5<sup>12</sup>6<sup>4</sup>*, J. Comput. Chem. **36**, 853 (2015).
- [161] S. Höfener, M. Trumm, C. Koke, J. Heuser, U. Ekström, A. Skerencak-Frech, B. Schimmelpfennig, and P. J. Panak, *Computing UV/vis spectra using a combined molecular dynamics and quantum chemistry approach: bis-triazin-pyridine (BTP) ligands studied in solution*, Phys. Chem. Chem. Phys. **18**, 7728 (2016).
- [162] M. Olejniczak, R. Bast, and A. S. P. Gomes, *On the calculation of second-order magnetic properties using subsystem approaches in a relativistic framework*, Phys. Chem. Chem. Phys. **19**, 8400 (2017).
- [163] F. E. Wolff, S. Höfener, M. Elstner, and T. A. Wesolowski, *Origin of the Solvatochromism in Organic Fluorophores with Flexible Side Chains: A Case Study of Flugi-2*, J. Phys. Chem. A **123**, 4581 (2019).
- [164] F. Egidi, S. Angelico, P. Lafiosca, T. Giovannini, and C. Cappelli, *A polarizable three-layer frozen density embedding/molecular mechanics approach*, J. Chem. Phys. **154**, 164107 (2021).
- [165] M. Humbert-Droz, X. Zhou, S. V. Shedge, and T. A. Wesolowski, *How to choose the frozen density in Frozen-Density Embedding Theory-based numerical simulations of local excitations?*, Theor. Chem. Acc. **133**, 1 (2014).

- [166] N. Ricardi, A. Zech, Y. Gimbal-Zofka, and T. A. Wesolowski, *Explicit vs. implicit electronic polarisation of environment of an embedded chromophore in frozen-density embedding theory*, Phys. Chem. Chem. Phys. **20**, 26053 (2018).
- [167] N. Ricardi, M. Ernst, P. Macchi, and T. A. Wesolowski, *Embedding-theory-based simulations using experimental electron densities for the environment*, Acta Cryst. A **76**, 571 (2020).
- [168] A. Laktionov, E. Chemineau-Chalaye, and T. A. Wesolowski, *Frozen-density embedding theory with average solvent charge densities from explicit atomistic simulations*, **18**, 21069 (2016).
- [169] N. Ricardi, C. E. González-Espinoza, S. Adam, J. Church, I. Schapiro, and T. A. Wesolowski, *Embedding non-rigid solutes in an averaged environment: a case study on rhodopsins*, (2021).
- [170] C. E. González-Espinoza, C. A. Rumble, D. Borgis, and T. A. Wesolowski, *Quantifying Fluctuations of Average Solvent Environments for Embedding Calculations*, J. Chem. Theory Comput. **18**, 1072 (2022).
- [171] A. Kovalenko and F. Hirata, *Self-consistent description of a metal–water interface by the Kohn–Sham density functional theory and the three-dimensional reference interaction site model*, J. Chem. Phys. **110**, 10095 (1999).
- [172] S. Gusarov, T. Ziegler, and A. Kovalenko, *Self-Consistent Combination of the Three-Dimensional RISM Theory of Molecular Solvation with Analytical Gradients and the Amsterdam Density Functional Package*, J. Phys. Chem. A **110**, 6083 (2006).
- [173] J. W. Kaminski, S. Gusarov, T. A. Wesolowski, and A. Kovalenko, *Modeling Solvatochromic Shifts Using the Orbital-Free Embedding Potential at Statistically Mechanically Averaged Solvent Density*, J. Phys. Chem. A **114**, 6082 (2010).

- [174] X. Zhou, J. W. Kaminski, and T. A. Wesolowski, *Multi-scale modelling of solvatochromic shifts from frozen-density embedding theory with non-uniform continuum model of the solvent: the coumarin 153 case*, *Phys. Chem. Chem. Phys.* **13**, 10565 (2011).
- [175] S. V. Shedge and T. A. Wesolowski, *Nonuniform Continuum Model for Solvatochromism Based on Frozen-Density Embedding Theory*, *ChemPhysChem* **15**, 3291 (2014).
- [176] S. V. Shedge, X. Zhou, and T. A. Wesolowski, *Non-uniform Continuum Model for Solvated Species Based on Frozen-Density Embedding Theory: The Study Case of Solvatochromism of Coumarin 153*, *Chimia* **68**, 609 (2014).
- [177] M. Bensberg, P. L. Türtscher, J. P. Unsleber, M. Reiher, and J. Neugebauer, *Solvation Free Energies in Subsystem Density Functional Theory*, *J. Chem. Theory Comput.* **18**, 723 (2022).
- [178] M. Iannuzzi, B. Kirchner, and J. Hutter, *Density functional embedding for molecular systems*, *Chem. Phys. Lett.* **421**, 16 (2006).
- [179] S. Kumar P., A. Genova, and M. Pavanello, *Cooperation and Environment Characterize the Low-Lying Optical Spectrum of Liquid Water*, *J. Phys. Chem. Lett.* **8**, 5077 (2017).
- [180] W. Mi, P. Ramos, J. Maranhao, and M. Pavanello, *Ab Initio Structure and Dynamics of CO<sub>2</sub> at Supercritical Conditions*, *J. Phys. Chem. Lett.* **10**, 7554 (2019).
- [181] A. Umerbekova and M. Pavanello, *Many-body response of benzene at monolayer MoS<sub>2</sub>: Van der Waals interactions and spectral broadening*, *Int. J. Quantum Chem.* **120**, e26243 (2020).
- [182] X. Shao, A. Umerbekova, K. Jiang, and M. Pavanello, *Many-body van der Waals interactions in wet MoS<sub>2</sub> surfaces*, *Electron. Struct.* **4**, 024001 (2022).

- [183] M. Pauletti, V. V. Rybkin, and M. Iannuzzi, *Subsystem Density Functional Theory Augmented by a Delta Learning Approach to Achieve Kohn–Sham Accuracy*, J. Chem. Theory Comput. **17**, 6423 (2021).
- [184] J. Behler, *Atom-centered symmetry functions for constructing high-dimensional neural network potentials*, J. Chem. Phys. **134**, 074106 (2011).
- [185] S. Lubner, *Local electric dipole moments for periodic systems via density functional theory embedding*, J. Chem. Phys. **141**, 234110 (2014).
- [186] M. Thomas, M. Brehm, R. Fligg, P. Vöhringer, and B. Kirchner, *Computing vibrational spectra from ab initio molecular dynamics*, Phys. Chem. Chem. Phys. **15**, 6608 (2013).
- [187] L. Schreder and S. Lubner, *Local approaches for electric dipole moments in periodic systems and their application to real-time time-dependent density functional theory*, J. Chem. Phys. **155**, 134116 (2021).
- [188] M. Mališ and S. Lubner,  *$\Delta$ SCF with Subsystem Density Embedding for Efficient Nonadiabatic Molecular Dynamics in Condensed-Phase Systems*, J. Chem. Theory Comput. **17**, 1653 (2021).
- [189] X. Shao, A. C. Lopez, M. R. Khan Musa, M. R. Nouri, and M. Pavanello, *Adaptive Subsystem Density Functional Theory*, J. Chem. Theory Comput. **18**, 6646 (2022).
- [190] A. Umerbekova, S.-F. Zhang, S. Kumar P., and M. Pavanello, *Dissecting energy level renormalization and polarizability enhancement of molecules at surfaces with subsystem TDDFT*, Eur. Phys. J. B **91**, 214 (2018).
- [191] X. Shao, W. Mi, and M. Pavanello, *Density Embedding Method for Nanoscale Molecule–Metal Interfaces*, J. Phys. Chem. Lett. **13**, 7147 (2022).

- [192] K. Fink and S. Höfener, *Combining wavefunction frozen-density embedding with one-dimensional periodicity*, J. Chem. Phys. **154**, 104114 (2021).
- [193] M. T. Wachter-Lehn, K. Fink, and S. Höfener, *Wavefunction frozen-density embedding with one-dimensional periodicity: Electronic polarization effects from local perturbations*, J. Chem. Phys. **157**, 134109 (2022).
- [194] F. Libisch, C. Huang, P. Liao, M. Pavone, and E. A. Carter, *Origin of the Energy Barrier to Chemical Reactions of O<sub>2</sub> on Al(111): Evidence for Charge Transfer, Not Spin Selection*, Phys. Rev. Lett. **109**, 198303 (2012).
- [195] Q. Zhao and E. A. Carter, *Revisiting Competing Paths in Electrochemical CO<sub>2</sub> Reduction on Copper via Embedded Correlated Wavefunction Theory*, J. Chem. Theory Comput. **16**, 6528 (2020).
- [196] Q. Zhao, J. M. P. Martirez, and E. A. Carter, *Revisiting Understanding of Electrochemical CO<sub>2</sub> Reduction on Cu(111): Competing Proton-Coupled Electron Transfer Reaction Mechanisms Revealed by Embedded Correlated Wavefunction Theory*, J. Am. Chem. Soc. **143**, 6152 (2021).
- [197] Q. Zhao, J. M. P. Martirez, and E. A. Carter, *Electrochemical Hydrogenation of CO on Cu(100): Insights from Accurate Multiconfigurational Wavefunction Methods*, J. Phys. Chem. Lett. **13**, 10282 (2022).
- [198] B. O. Roos, *The complete active space SCF method in a fock-matrix-based super-CI formulation*, Int. J. Quantum Chem. **18**, 175 (1980).
- [199] K. Andersson, P. Å. Malmqvist, B. O. Roos, A. J. Sadlej, and K. Wolinski, *Second-order perturbation theory with a CASSCF reference function*, J. Phys. Chem. **94**, 5483 (1990).

- [200] N. M. Tubman, J. Lee, T. Y. Takeshita, M. Head-Gordon, and K. B. Whaley, *A deterministic alternative to the full configuration interaction quantum Monte Carlo method*, *J. Chem. Phys.* **145**, 044112 (2016).
- [201] J. Tölle, A. Severo Pereira Gomes, P. Ramos, and M. Pavanello, *Charged-cell periodic DFT simulations via an impurity model based on density embedding: Application to the ionization potential of liquid water*, *Int. J. Quantum Chem.* **119**, e25801 (2019).
- [202] J. A. Martinez B, L. Paetow, J. Tölle, X. Shao, P. Ramos, J. Neugebauer, and M. Pavanello, *Which Physical Phenomena Determine the Ionization Potential of Liquid Water?*, *J. Phys. Chem. B* **127**, 5470 (2023).
- [203] R. A. Opoku, C. Toubin, and A. S. P. Gomes, *Simulating core electron binding energies of halogenated species adsorbed on ice surfaces and in solution via relativistic quantum embedding calculations*, *Phys. Chem. Chem. Phys.* **24**, 14390 (2022).
- [204] D. W. Zhang and J. Z. H. Zhang, *Molecular fractionation with conjugate caps for full quantum mechanical calculation of protein–molecule interaction energy*, *J. Chem. Phys.* **119**, 3599 (2003).
- [205] J. Liu, T. Zhu, X. He, and J. Z. H. Zhang, MFCC-Based Fragmentation Methods for Biomolecules, in *Fragmentation*, pages 323–348, John Wiley & Sons, Ltd, 2017.
- [206] K. Kiewisch, Ch. R. Jacob, and L. Visscher, *Quantum-Chemical Electron Densities of Proteins and of Selected Protein Sites from Subsystem Density Functional Theory*, *J. Chem. Theory Comput.* **9**, 2425 (2013).
- [207] A. Goez and J. Neugebauer, *Benchmarking Electron Densities and Electrostatic Potentials of Proteins from the Three-Partition Frozen Density Embedding Method*, *J. Chem. Theory Comput.* **12**, 4843 (2016).

- [208] A. Goez, Ch. R. Jacob, and J. Neugebauer, *Modeling environment effects on pigment site energies: Frozen density embedding with fully quantum-chemical protein densities*, *Comput. Theor. Chem.* **1040–1041**, 347 (2014).
- [209] A. Goez and J. Neugebauer, *Including protein density relaxation effects in first-principles embedding calculations of cofactor excitation energies*, *Mol. Phys.* **115**, 526 (2017).
- [210] A. Goez and J. Neugebauer, *A Local Variant of the Conductor-Like Screening Model for Fragment-Based Electronic-Structure Methods*, *J. Chem. Theory Comput.* **11**, 5277 (2015).
- [211] M. von Looz, M. Wolter, Ch. R. Jacob, and H. Meyerhenke, *Better Partitions of Protein Graphs for Subsystem Quantum Chemistry*, in *Experimental Algorithms*, edited by A. V. Goldberg and A. S. Kulikov, *Lecture Notes in Computer Science*, pages 353–368, Springer International Publishing, 2016, DOI: 10.1007/978-3-319-38851-9\_24.
- [212] X. Zhou, D. Sundholm, T. A. Wesółowski, and V. R. I. Kaila, *Spectral Tuning of Rhodopsin and Visual Cone Pigments*, *J. Am. Chem. Soc.* **136**, 2723 (2014).
- [213] J. Heuser and S. Höfener, *Communication: Biological applications of coupled-cluster frozen-density embedding*, *J. Chem. Phys.* **148**, 141101 (2018).
- [214] P. K. Tamukong, Y. G. Khait, and M. R. Hoffmann, *Accurate Dissociation of Chemical Bonds Using DFT-in-DFT Embedding Theory with External Orbital Orthogonality*, *J. Phys. Chem. A* **121**, 256 (2017).
- [215] F. R. Manby, M. Stella, J. D. Goodpaster, and T. F. Miller, *A Simple, Exact Density-Functional-Theory Embedding Scheme*, *J. Chem. Theory Comput.* **8**, 2564 (2012).

- [216] B. Hégyely, P. R. Nagy, G. G. Ferenczy, and M. Kállay, *Exact density functional and wave function embedding schemes based on orbital localization*, J. Chem. Phys. **145**, 064107 (2016).
- [217] S. Huzinaga and A. A. Cantu, *Theory of Separability of Many-Electron Systems*, J. Chem. Phys. **55**, 5543 (1971).
- [218] N. Niemeyer, J. Tölle, and J. Neugebauer, *Approximate versus Exact Embedding for Chiroptical Properties: Reconsidering Failures in Potential and Response*, J. Chem. Theory Comput. **16**, 3104 (2020).
- [219] J. M. H. Olsen, C. Steinmann, K. Ruud, and J. Kongsted, *Polarizable Density Embedding: A New QM/QM/MM-Based Computational Strategy*, J. Phys. Chem. A **119**, 5344 (2015).
- [220] P. Reinholdt, J. Kongsted, and J. M. H. Olsen, *Polarizable Density Embedding: A Solution to the Electron Spill-Out Problem in Multiscale Modeling*, J. Phys. Chem. Lett. , 5949 (2017).
- [221] P. P. Pal, P. Liu, and L. Jensen, *Polarizable Frozen Density Embedding with External Orthogonalization*, J. Chem. Theory Comput. **15**, 6588 (2019).
- [222] T. Culpitt, K. R. Brorsen, and S. Hammes-Schiffer, *Communication: Density functional theory embedding with the orthogonality constrained basis set expansion procedure*, J. Chem. Phys. **146**, 211101 (2017).
- [223] W. J. Hunt, T. H. Dunning, and W. A. Goddard, *The orthogonality constrained basis set expansion method for treating off-diagonal lagrange multipliers in calculations of electronic wave functions*, Chem. Phys. Lett. **3**, 606 (1969).
- [224] G. Marrazzini, T. Giovannini, M. Scavino, F. Egidi, C. Cappelli, and H. Koch, *Multilevel Density Functional Theory*, J. Chem. Theory Comput. **17**, 791 (2021).

- [225] T. Giovannini, G. Marrazzini, M. Scavino, H. Koch, and C. Cappelli, *Integrated Multiscale Multilevel Approach to Open Shell Molecular Systems*, *J. Chem. Theory Comput.* **19**, 1446 (2023).
- [226] S. Sæther, T. Kjærgaard, H. Koch, and I.-M. Høyvik, *Density-Based Multilevel Hartree–Fock Model*, *J. Chem. Theory Comput.* **13**, 5282–5290 (2017).
- [227] T. A. Barnes, J. D. Goodpaster, F. R. Manby, and T. F. M. Iii, *Accurate basis set truncation for wavefunction embedding*, *J. Chem. Phys.* **139**, 024103 (2013).
- [228] S. J. Bennie, M. Stella, T. F. M. Iii, and F. R. Manby, *Accelerating wavefunction in density-functional-theory embedding by truncating the active basis set*, *J. Chem. Phys.* **143**, 024105 (2015).
- [229] M. Bensberg and J. Neugebauer, *Automatic basis-set adaptation in projection-based embedding*, *J. Chem. Phys.* **150**, 184104 (2019).
- [230] M. Bensberg and J. Neugebauer, *Erratum: “Automatic basis-set adaptation in projection-based embedding” [*J. Chem. Phys.* 150, 184104 (2019)]*, *J. Chem. Phys.* **151**, 139903 (2019).
- [231] B. Hégyely, P. R. Nagy, and M. Kállay, *Dual Basis Set Approach for Density Functional and Wave Function Embedding Schemes*, *J. Chem. Theory Comput.* **14**, 4600 (2018).
- [232] M. Bensberg and J. Neugebauer, *Direct orbital selection for projection-based embedding*, *J. Chem. Phys.* **150**, 214106 (2019).
- [233] M. A. Iron and T. Janes, *Evaluating Transition Metal Barrier Heights with the Latest Density Functional Theory Exchange–Correlation Functionals: The MOBH35 Benchmark Database*, *J. Phys. Chem. A* **123**, 3761 (2019).

- [234] Z. Amanollahi, L. Lampe, M. Bensberg, J. Neugebauer, and M. Feldt, *On the accuracy of orbital based multi-level approaches for closed-shell transition metal chemistry*, Phys. Chem. Chem. Phys. **25**, 4635 (2023).
- [235] D. Claudino and N. J. Mayhall, *Automatic Partition of Orbital Spaces Based on Singular Value Decomposition in the Context of Embedding Theories*, J. Chem. Theory Comput. **15**, 1053 (2019).
- [236] D. Claudino and N. J. Mayhall, *Simple and Efficient Truncation of Virtual Spaces in Embedded Wave Functions via Concentric Localization*, J. Chem. Theory Comput. **15**, 6085 (2019).
- [237] M. Bensberg and J. Neugebauer, *Orbital Alignment for Accurate Projection-Based Embedding Calculations along Reaction Paths*, J. Chem. Theory Comput. **16**, 3607 (2020).
- [238] M. Bensberg and J. Neugebauer, *Direct orbital selection within the domain-based local pair natural orbital coupled-cluster method*, J. Chem. Phys. **155**, 224102 (2021).
- [239] M. Welborn, F. R. Manby, and T. F. Miller, *Even-handed subsystem selection in projection-based embedding*, J. Chem. Phys. **149**, 144101 (2018).
- [240] D. V. Chulhai and J. D. Goodpaster, *Improved Accuracy and Efficiency in Quantum Embedding through Absolute Localization*, J. Chem. Theory Comput. **13**, 1503 (2017).
- [241] D. S. Graham, X. Wen, D. V. Chulhai, and J. D. Goodpaster, *Robust, Accurate, and Efficient: Quantum Embedding Using the Huzinaga Level-Shift Projection Operator for Complex Systems*, J. Chem. Theory Comput. **16**, 2284 (2020).
- [242] H. R. Petras, D. S. Graham, S. K. Ramadugu, J. D. Goodpaster, and J. J. Shepherd, *Fully Quantum Embedding with Density Functional Theory for Full Configuration Interaction Quantum Monte Carlo*, J. Chem. Theory Comput. **15**, 5332 (2019).

- [243] D. S. Graham, X. Wen, D. V. Chulhai, and J. D. Goodpaster, *Huzinaga projection embedding for efficient and accurate energies of systems with localized spin-densities*, J. Chem. Phys. **156**, 054112 (2022).
- [244] A. Cembran, L. Song, Y. Mo, and J. Gao, *Block-Localized Density Functional Theory (BLDFT), Diabatic Coupling, and Their Use in Valence Bond Theory for Representing Reactive Potential Energy Surfaces*, J. Chem. Theory Comput. **5**, 2702 (2009).
- [245] Y. Mo and S. D. Peyerimhoff, *Theoretical analysis of electronic delocalization*, J. Chem. Phys. **109**, 1687 (1998).
- [246] J. D. Goodpaster, T. A. Barnes, F. R. Manby, and T. F. Miller, *Accurate and systematically improvable density functional theory embedding for correlated wavefunctions*, J. Chem. Phys. **140**, 18A507 (2014).
- [247] P. Beran, K. Pernal, F. Pavošević, and L. Veis, *Projection-Based Density Matrix Renormalization Group in Density Functional Theory Embedding*, J. Phys. Chem. Lett. **14**, 716 (2023).
- [248] S. J. R. Lee, F. Ding, F. R. Manby, and T. F. Miller, *Analytical gradients for projection-based wavefunction-in-DFT embedding*, J. Chem. Phys. **151**, 064112 (2019).
- [249] R. C. R. Pennifold, S. J. Bennie, T. F. M. III, and F. R. Manby, *Correcting density-driven errors in projection-based embedding*, J. Chem. Phys. **146**, 084113 (2017).
- [250] D. V. Chulhai and J. D. Goodpaster, *Projection-Based Correlated Wave Function in Density Functional Theory Embedding for Periodic Systems*, J. Chem. Theory Comput. **14**, 1928 (2018).
- [251] F. Pavošević and A. Rubio, *Wavefunction embedding for molecular polaritons*, J. Chem. Phys. **157**, 094101 (2022).

- [252] M. Stella, S. J. Bennie, and F. R. Manby, *Computational study of adsorption of cobalt on benzene and coronene*, Mol. Phys. **113**, 1858 (2015).
- [253] P. Huo, C. Uyeda, J. D. Goodpaster, J. C. Peters, and T. F. I. Miller, *Breaking the Correlation between Energy Costs and Kinetic Barriers in Hydrogen Evolution via a Cobalt Pyridine-Diimine-Dioxime Catalyst*, ACS Catalysis **6**, 6114 (2016).
- [254] A. Chapovetsky, M. Welborn, J. M. Luna, R. Haiges, T. F. I. Miller, and S. C. Marinescu, *Pendant Hydrogen-Bond Donors in Cobalt Catalysts Independently Enhance CO<sub>2</sub> Reduction*, ACS Cent. Sci. **4**, 397 (2018).
- [255] S. J. Bennie, M. W. van der Kamp, R. C. R. Pennifold, M. Stella, F. R. Manby, and A. J. Mulholland, *A Projector-Embedding Approach for Multiscale Coupled-Cluster Calculations Applied to Citrate Synthase*, J. Chem. Theory Comput. **12**, 2689 (2016).
- [256] X. Zhang, S. J. Bennie, M. W. van der Kamp, D. R. Glowacki, F. R. Manby, and A. J. Mulholland, *Multiscale analysis of enantioselectivity in enzyme-catalysed ‘lethal synthesis’ using projector-based embedding*, R. Soc. Open Sci **5**, 171390 (2018).
- [257] T. A. Barnes, J. W. Kaminski, O. Borodin, and T. F. I. Miller, *Ab Initio Characterization of the Electrochemical Stability and Solvation Properties of Condensed-Phase Ethylene Carbonate and Dimethyl Carbonate Mixtures*, J. Phys. Chem. C **119**, 3865 (2015).
- [258] A. P. d. L. Batista, A. G. S. d. Oliveira-Filho, and S. E. Galembeck, *Photophysical properties and the NO photorelease mechanism of a ruthenium nitrosyl model complex investigated using the CASSCF-in-DFT embedding approach*, Phys. Chem. Chem. Phys. **19**, 13860 (2017).

- [259] M. Leopoldini, N. Russo, M. Toscano, M. Dulak, and T. A. Wesolowski, *Mechanism of Nitrate Reduction by Desulfovibrio desulfuricans Nitrate Reductase - A Theoretical Investigation*, Chem. Eur. J. **12**, 2532 (2006).
- [260] C. Daday, C. König, O. Valsson, J. Neugebauer, and C. Filippi, *State-Specific Embedding Potentials for Excitation-Energy Calculations*, J. Chem. Theory Comput. **9**, 2355 (2013).
- [261] C. Daday, C. König, J. Neugebauer, and C. Filippi, *Wavefunction in Density Functional Theory Embedding for Excited States: Which Wavefunctions, which Densities?*, ChemPhysChem **15**, 3205 (2014).
- [262] A. Solovyeva, M. Pavanello, and J. Neugebauer, *Describing long-range charge-separation processes with subsystem density-functional theory*, J. Chem. Phys. **140**, 164103 (2014).
- [263] Y. G. Khait and M. R. Hoffmann, *Embedding theory for excited states*, J. Chem. Phys. **133**, 044107 (2010).
- [264] C. Daday, C. Curutchet, A. Sinicropi, B. Mennucci, and C. Filippi, *Chromophore-Protein Coupling beyond Nonpolarizable Models: Understanding Absorption in Green Fluorescent Protein*, J. Chem. Theory Comput. **11**, 4825 (2015).
- [265] T. A. Wesolowski, *Embedding potentials for excited states of embedded species*, J. Chem. Phys. **140**, 18A530 (2014).
- [266] J. Tölle and J. Neugebauer, *The Seamless Connection of Local and Collective Excited States in Subsystem Time-Dependent Density Functional Theory*, J. Phys. Chem. Lett. **13**, 1003 (2022).
- [267] J. Tölle and J. Neugebauer, *Correction to “The Seamless Connection of Local and Collective Excited States in Subsystem Time-Dependent Density Functional Theory”*, J. Phys. Chem. Lett. **13**, 1742 (2022).

- [268] J. Tölle, M. Böckers, N. Niemeyer, and J. Neugebauer, *Inter-subsystem charge-transfer excitations in exact subsystem time-dependent density-functional theory*, J. Chem. Phys. **151**, 174109 (2019).
- [269] M. Böckers and J. Neugebauer, *Excitation energies of embedded open-shell systems: Unrestricted frozen-density-embedding time-dependent density-functional theory*, J. Chem. Phys. **149**, 074102 (2018).
- [270] C. König, N. Schlüter, and J. Neugebauer, *Direct determination of exciton couplings from subsystem time-dependent density-functional theory within the Tamm–Dancoff approximation*, J. Chem. Phys. **138**, 034104 (2013).
- [271] R. S. Treß, C. Hättig, and S. Höfener, *Employing Pseudopotentials to Tackle Excited-State Electron Spill-Out in Frozen Density Embedding Calculations*, J. Chem. Theory Comput. **18**, 1737 (2022).
- [272] A. M. Khah, P. Reinholdt, J. M. H. Olsen, J. Kongsted, and C. Hättig, *Avoiding Electron Spill-Out in QM/MM Calculations on Excited States with Simple Pseudopotentials*, J. Chem. Theory Comput. (2020).
- [273] J. Tölle, M. Böckers, and J. Neugebauer, *Exact subsystem time-dependent density-functional theory*, J. Chem. Phys. **150**, 181101 (2019).
- [274] D. V. Chulhai and L. Jensen, *External orthogonality in subsystem time-dependent density functional theory*, **18**, 21032 (2016).
- [275] J. Tölle, L. Cupellini, B. Mennucci, and J. Neugebauer, *Electronic couplings for photo-induced processes from subsystem time-dependent density-functional theory: The role of the diabaticization*, J. Chem. Phys. **153**, 184113 (2020).
- [276] L. Scholz, J. Tölle, and J. Neugebauer, *Analysis of environment response effects on excitation energies within subsystem-based time-dependent density-functional theory*, Int. J. Quantum Chem. **120**, e26213 (2020).

- [277] P. Eschenbach, N. Niemeyer, and J. Neugebauer, *Massively parallel fragment-based quantum chemistry for large molecular systems: the serestipy software*, *Can. J. Chem.* (2023).
- [278] S. Sen, B. Senjean, and L. Visscher, *Characterization of excited states in time-dependent density functional theory using localized molecular orbitals*, *J. Chem. Phys.* **158**, 054115 (2023).
- [279] S. J. Bennie, B. F. E. Curchod, F. R. Manby, and D. R. Glowacki, *Pushing the Limits of EOM-CCSD with Projector-Based Embedding for Excitation Energies*, *J. Phys. Chem. Lett.* **8**, 5559 (2017).
- [280] V. Parravicini and T.-C. Jagau, *Embedded equation-of-motion coupled-cluster theory for electronic excitation, ionisation, electron attachment, and electronic resonances*, *Mol. Phys.* **119**, e1943029 (2021).
- [281] X. Wen, D. S. Graham, D. V. Chulhai, and J. D. Goodpaster, *Absolutely Localized Projection-Based Embedding for Excited States*, *J. Chem. Theory Comput.* **16**, 385 (2020).
- [282] A. Kovyrshin and J. Neugebauer, *Analytical gradients for excitation energies from frozen-density embedding*, **18**, 20955 (2016).
- [283] J. Heuser and S. Höfener, *Wave-function frozen-density embedding: Approximate analytical nuclear ground-state gradients*, *J. Comput. Chem.* **37**, 1092 (2016).
- [284] J. Heuser and S. Höfener, *Analytical nuclear excited-state gradients for the Tamm–Dancoff approximation using uncoupled frozen-density embedding*, *J. Comput. Chem.* **38**, 2316 (2017).
- [285] J. Heuser and S. Höfener, *Analytical Nuclear Excited-State Gradients for the Second-Order Approximate Coupled-Cluster Singles and Doubles (CC2) Method Employing Uncoupled Frozen-Density Embedding*, *J. Chem. Theory Comput.* **14**, 4616 (2018).

- [286] J. Liu, C. Hättig, and S. Höfener, *Analytical nuclear gradients for electron-attached and electron-detached states for the second-order algebraic diagrammatic construction scheme combined with frozen-density embedding*, J. Chem. Phys. **152**, 174109 (2020).
- [287] C. Huang, F. Libisch, Q. Peng, and E. A. Carter, *Time-dependent potential-functional embedding theory*, J. Chem. Phys. **140**, 124113 (2014).
- [288] A. Krishtal and M. Pavanello, *Revealing electronic open quantum systems with subsystem TDDFT*, J. Chem. Phys. **144**, 124118 (2016).
- [289] M. De Santis, L. Belpassi, Ch. R. Jacob, A. Severo Pereira Gomes, F. Tarantelli, L. Visscher, and L. Storchi, *Environmental Effects with Frozen-Density Embedding in Real-Time Time-Dependent Density Functional Theory Using Localized Basis Functions*, J. Chem. Theory Comput. **16**, 5695 (2020).
- [290] Ch. R. Jacob, S. M. Beyhan, R. E. Bulo, A. S. P. Gomes, A. W. Götz, K. Kiewisch, J. Sikkema, and L. Visscher, *PyADF — A scripting framework for multiscale quantum chemistry*, J. Comput. Chem. **32**, 2328 (2011).
- [291] D. G. A. Smith et al., *Psi4 1.4: Open-source software for high-throughput quantum chemistry*, J. Chem. Phys. **152**, 184108 (2020).
- [292] D. G. A. Smith et al., *Psi4NumPy: An Interactive Quantum Chemistry Programming Environment for Reference Implementations and Rapid Development*, J. Chem. Theory Comput. **14**, 3504 (2018).
- [293] G. te Velde, F. M. Bickelhaupt, E. J. Baerends, C. Fonseca Guerra, S. J. A. van Gisbergen, J. G. Snijders, and T. Ziegler, *Chemistry with ADF*, J. Comput. Chem. **22**, 931 (2001).
- [294] Software for Chemistry and Materials, Amsterdam, AMS, Amsterdam Modelling Suite, 2020, URL: <http://www.scm.com>.

- [295] H. Ren, M. R. Provorse, P. Bao, Z. Qu, and J. Gao, *Multistate Density Functional Theory for Effective Diabatic Electronic Coupling*, J. Phys. Chem. Lett. **7**, 2286 (2016).
- [296] Q. Wu, C.-L. Cheng, and T. Van Voorhis, *Configuration interaction based on constrained density functional theory: A multireference method*, J. Chem. Phys. **127**, 164119 (2007).
- [297] P. Ramos, M. Papadakis, and M. Pavanello, *Performance of Frozen Density Embedding for Modeling Hole Transfer Reactions*, J. Phys. Chem. B **119**, 7541 (2015).
- [298] F. Hernández-Fernández, M. Pavanello, and L. Visscher, *Effect of metallation, substituents and inter/intra-molecular polarization on electronic couplings for hole transport in stacked porphyrin dyads*, Phys. Chem. Chem. Phys. **18**, 21122 (2016).
- [299] P. Ramos and M. Pavanello, *Quantifying Environmental Effects on the Decay of Hole Transfer Couplings in Biosystems*, J. Chem. Theory Comput. **10**, 2546 (2014).
- [300] G. Hong, R. Pachter, L.-O. Essen, and T. Ritz, *Electron transfer and spin dynamics of the radical-pair in the cryptochrome from *Chlamydomonas reinhardtii* by computational analysis*, J. Chem. Phys. **152**, 065101 (2020).
- [301] C. Schober, K. Reuter, and H. Oberhofer, *Critical analysis of fragment-orbital DFT schemes for the calculation of electronic coupling values*, J. Chem. Phys. **144**, 054103 (2016).
- [302] D. G. Artiukhin and J. Neugebauer, *Frozen-density embedding as a quasi-diabatization tool: Charge-localized states for spin-density calculations*, J. Chem. Phys. **148**, 214104 (2018).
- [303] P. Eschenbach, D. G. Artiukhin, and J. Neugebauer, *Multi-state formulation of the frozen-density embedding quasi-diabatization approach*, J. Chem. Phys. **155**, 174104 (2021).

- [304] D. G. Artiukhin, P. Eschenbach, and J. Neugebauer, *Computational Investigation of the Spin-Density Asymmetry in Photosynthetic Reaction Center Models from First Principles*, J. Phys. Chem. B **124**, 4873 (2020).
- [305] D. G. Artiukhin, P. Eschenbach, J. Matysik, and J. Neugebauer, *Theoretical Assessment of Hinge-Type Models for Electron Donors in Reaction Centers of Photosystems I and II as well as of Purple Bacteria*, J. Phys. Chem. B **125**, 3066 (2021).
- [306] P. Ramos and M. Pavanello, *Constrained subsystem density functional theory*, Phys. Chem. Chem. Phys. **18**, 21172 (2016).
- [307] J. Neugebauer, *On the calculation of general response properties in subsystem density functional theory*, J. Chem. Phys. **131**, 084104 (2009).
- [308] T. D. Crawford, A. Kumar, K. P. Hannon, S. Höfener, and L. Visscher, *Frozen-Density Embedding Potentials and Chiroptical Properties*, J. Chem. Theory Comput. **11**, 5305 (2015).
- [309] M. Caricato, *Origin invariant optical rotation in the length dipole gauge without London atomic orbitals*, J. Chem. Phys. **153**, 151101 (2020).
- [310] A. K. Harshan, M. J. Bronson, and L. Jensen, *Local-Field Effects in Linear Response Properties within a Polarizable Frozen Density Embedding Method*, J. Chem. Theory Comput. **18**, 380 (2022).
- [311] Ch. R. Jacob and L. Visscher, *Calculation of nuclear magnetic resonance shieldings using frozen-density embedding*, J. Chem. Phys. **125**, 194104 (2006).
- [312] A. W. Götz, J. Autschbach, and L. Visscher, *Calculation of nuclear spin-spin coupling constants using frozen density embedding*, J. Chem. Phys. **140**, 104107 (2014).

- [313] R. Kevorkyants, X. Wang, D. M. Close, and M. Pavanello, *Calculating Hyperfine Couplings in Large Ionic Crystals Containing Hundreds of QM Atoms: Subsystem DFT Is the Key*, J. Phys. Chem. B **117**, 13967 (2013).
- [314] T. A. Wesolowski, *Embedding a multideterminantal wave function in an orbital-free environment*, Phys. Rev. A **77**, 012504 (2008).
- [315] A. Zech, A. Dreuw, and T. A. Wesolowski, *Extension of frozen-density embedding theory for non-variational embedded wavefunctions*, J. Chem. Phys. **150**, 121101 (2019).
- [316] T. A. Wesolowski, *On the Correlation Potential in Frozen-Density Embedding Theory*, J. Chem. Theory Comput. **16**, 6880 (2020).
- [317] R. Sen, C. E. González-Espinoza, A. Zech, A. Dreuw, and T. A. Wesolowski, *Benchmark of the Extension of Frozen-Density Embedding Theory to Nonvariational Correlated Methods: The Embedded-MP2 Case*, J. Chem. Theory Comput. **17**, 4049 (2021).
- [318] T. Dresselhaus, J. Neugebauer, S. Knecht, S. Keller, Y. Ma, and M. Reiher, *Self-consistent embedding of density-matrix renormalization group wavefunctions in a density functional environment*, J. Chem. Phys. **142**, 044111 (2015).
- [319] T. Dresselhaus, J. Neugebauer, S. Knecht, S. Keller, Y. Ma, and M. Reiher, *Erratum: “Self-consistent embedding of density-matrix renormalization group wavefunctions in a density functional environment” [J. Chem. Phys. 142, 044111 (2015)]*, J. Chem. Phys. **142**, 189901 (2015).
- [320] A. Zech, F. Aquilante, and T. A. Wesolowski, *Orthogonality of embedded wave functions for different states in frozen-density embedding theory*, J. Chem. Phys. **143**, 164106 (2015).

- [321] A. Zech, F. Aquilante, and T. A. Wesolowski, *Homogeneity properties of the embedding potential in frozen-density embedding theory*, Mol. Phys. **114**, 1199 (2016).
- [322] M. Fu and T. A. Wesolowski, *Excitation Energies of Embedded Chromophores from Frozen-Density Embedding Theory Using State-Specific Electron Densities of the Environment*, J. Phys. Chem. A **127**, 535 (2023).
- [323] S. Höfener, A. S. P. Gomes, and L. Visscher, *Solvatochromic shifts from coupled-cluster theory embedded in density functional theory*, J. Chem. Phys. **139**, 104106 (2013).
- [324] S. Höfener, *Coupled-cluster frozen-density embedding using resolution of the identity methods*, J. Comput. Chem. **35**, 1716 (2014).
- [325] S. Höfener and L. Visscher, *Wave Function Frozen-Density Embedding: Coupled Excitations*, J. Chem. Theory Comput. **12**, 549 (2016).
- [326] N. Schieschke, R. Di Remigio, L. Frediani, J. Heuser, and S. Höfener, *Combining frozen-density embedding with the conductor-like screening model using Lagrangian techniques for response properties*, J. Comput. Chem. **38**, 1693 (2017).
- [327] N. Schieschke, T. Bodenstein, and S. Höfener, *Frozen-density embedding employing configuration interaction as a subsystem method*, Mol. Phys. **118**, e1665726 (2020).
- [328] N. Schieschke, T. Bodenstein, and S. Höfener, *A Fock-operator complete active space self-consistent field (CAS-SCF) method combined with frozen-density embedding*, J. Chem. Phys. **154**, 084120 (2021).
- [329] J. Schirmer, *Beyond the random-phase approximation: A new approximation scheme for the polarization propagator*, Phys. Rev. A **26**, 2395 (1982).
- [330] S. Prager, A. Zech, F. Aquilante, A. Dreuw, and T. A. Wesolowski, *First time combination of frozen density embedding theory with the algebraic diagrammatic*

- construction scheme for the polarization propagator of second order*, J. Chem. Phys. **144**, 204103 (2016).
- [331] S. Prager, A. Zech, T. A. Wesolowski, and A. Dreuw, *Implementation and Application of the Frozen Density Embedding Theory with the Algebraic Diagrammatic Construction Scheme for the Polarization Propagator up to Third Order*, J. Chem. Theory Comput. **13**, 4711 (2017).
- [332] A. Zech, N. Ricardi, S. Prager, A. Dreuw, and T. A. Wesolowski, *Benchmark of Excitation Energy Shifts from Frozen-Density Embedding Theory: Introduction of a Density-Overlap-Based Applicability Threshold*, J. Chem. Theory Comput. **14**, 4028–4040 (2018).
- [333] B. Hégyely, Á. B. Szirmai, D. Mester, A. Tajti, P. G. Szalay, and M. Kállay, *Performance of Multilevel Methods for Excited States*, J. Phys. Chem. A **126**, 6548 (2022).
- [334] M. Fu and T. A. Wesolowski, *The Challenge of Accurate Computation of Two-Photon Absorption Properties of Organic Chromophores in the Condensed Phase*, J. Chem. Theory Comput. **17**, 3652 (2021).
- [335] J. Tölle, T. Deilmann, M. Rohlfing, and J. Neugebauer, *Subsystem-Based GW/Bethe–Salpeter Equation*, J. Chem. Theory Comput. **17**, 2186 (2021).
- [336] J. Tölle, T. Deilmann, M. Rohlfing, and J. Neugebauer, *Correction to “Subsystem-Based GW/Bethe–Salpeter Equation”*, J. Chem. Theory Comput. **19**, 2699 (2023).
- [337] F. Libisch, J. Cheng, and E. A. Carter, *Electron-Transfer-Induced Dissociation of H<sub>2</sub> on Gold Nanoparticles: Excited-State Potential Energy Surfaces via Embedded Correlated Wavefunction Theory*, Z. Phys. Chem. **227**, 1455 (2013).

- [338] J. M. P. Martirez and E. A. Carter, *Metal-to-Ligand Charge-Transfer Spectrum of a Ru-Bipyridine-Sensitized TiO<sub>2</sub> Cluster from Embedded Multiconfigurational Excited-State Theory*, J. Phys. Chem. A **125**, 4998 (2021).